Cross-validation of lipid structure assignment using orthogonal ion activation modalities on the same mass spectrometer

Samuel C. Brydon[a], Berwyck L.J. Poad[a,b], Mengxuan Fang[c], Yepy H. Rustam[d], Reuben S.E. Young[e], Dmitri Mouradov[f], Oliver M. Sieber[f], Todd W. Mitchell[g], Gavin E. Reid[c,d,h]*, Stephen J. Blanksby[a,b]*, and David L. Marshall[b]*

[a]*School of Chemistry and Physics, Queensland University of Technology, Brisbane, QLD 4001, Australia*
[b]*Central Analytical Research Facility, Queensland University of Technology, Brisbane, QLD 4001, Australia*
[c]*School of Chemistry, University of Melbourne, Parkville, VIC 3010, Australia*
[d]*Department of Biochemistry and Pharmacology, University of Melbourne, Parkville, VIC 3010, Australia*
[e]*Molecular Horizons and School of Chemistry and Molecular Bioscience, University of Wollongong, Wollongong, NSW 2522, Australia*
[f]*Personalized Oncology Division, The Walter and Eliza Hall Institute of Medical Research, Parkville, VIC 3052, Australia*
[g]*Molecular Horizons and School of Medical, Indigenous and Health Sciences, University of Wollongong, Wollongong, NSW 2522, Australia*
[h]*Bio21 Molecular Science and Biotechnology Institute, University of Melbourne, Parkville, VIC 3010, Australia*
*Email: gavin.reid@unimelb.edu.au, stephen.blanksby@qut.edu.au, d20.marshall@qut.edu.au

ABSTRACT: The onset and progression of cancer is associated with changes in the composition of the lipidome. Therefore, better understanding of the molecular mechanisms of these disease states requires detailed structural characterization of the individual lipids within the complex cellular milieu. Recently, changes in the unsaturation profile of membrane lipids have been observed in cancer cells and tissues, but assigning the position(s) of carbon-carbon double bonds in fatty acyl chains carried by membrane phospholipids, including the resolution of lipid regioisomers, has proven analytically challenging. Conventional tandem mass spectrometry approaches based on collision-induced dissociation of ionized glycerophospholipids do not yield spectra that are indicative of the location(s) of carbon-carbon double bonds. Ozone-induced dissociation (OzID) and ultraviolet photodissociation (UVPD) have emerged as alternative ion activation modalities wherein diagnostic product ions can enable *de novo* assignment of position(s) of unsaturation based on predictable fragmentation behaviors. Here, for the first time, OzID and UVPD (193 nm) mass spectra are acquired on the same mass spectrometer to evaluate the relative performance of the two modalities for lipid identification and to interrogate the respective fragmentation pathways under comparable conditions. Based on investigations of lipid standards, fragmentation rules for each technique are expanded to increase confidence in structural assignments and exclude potential false positives. Parallel application of both methods to unsaturated phosphatidylcholines extracted from isogenic colorectal cancer cell lines provides high confidence in the assignment of multiple double bond isomers in these samples and cross-validates relative changes in isomer abundance.

INTRODUCTION

Various human diseases including obesity, diabetes, and Alzheimer's disease are associated with changes in the cellular lipidome.[1-4] Cancer is another pathology that is adept at increasing cellular uptake and *de novo* synthesis of lipids in order to maintain rapid cell proliferation.[5-9] Consequently, detailed structural characterization of lipids in extracts from cancer cells and tissues is increasingly desirable and requires molecular identification based on lipid class, number of carbons and double bonds (sum composition), relative (*sn*-) position of fatty acyl chains in glycerolipids, and the position of functional groups on fatty acyl chains (*e.g.*, unsaturation, methylation, or hydroxylation). Establishing the sites(s) of unsaturation within glycerophospholipids has been a recent focus in cancer lipidomics due to observations of perturbations in desaturation and elongation metabolism[10, 11] that may potentiate downstream impacts on membrane biophysical properties (*e.g.*, lipid membrane fluidity).[12, 13] Determining the position(s) of carbon-carbon double bonds is thus central to understanding the variability of human lipid metabolism in health and disease; particularly those pathways involving the expression and activity of the three mammalian desaturase enzymes SCD-1, FADS1 and FADS2.[14, 15] Notably, changes in the relative abundance of *n*-7 and *n*-9 double bond isomers in glycerophospholipids have been found to be phenotypic of cancer,[16-19] while the recent observation of *n*-10 double bonds in some cancers is evidence for activation of FADS2 metabolism toward saturated fatty acids; a process first thought to be confined to human skin.[10, 20-23] Such discoveries have reinvigorated efforts to develop mass spectrometric techniques

capable of assigning double bond position(s) in glycerophospholipids (and other lipid classes).

Electrospray ionization-mass spectrometry (ESI-MS), using either direct infusion or coupled to liquid chromatography, has emerged as the most widely used method for lipid identification and quantification.[24, 25] In such lipidomics workflows, data including combinations of chromatographic retention time, accurate mass measurement and characteristic fragmentation upon tandem mass spectrometry (MS/MS) can provide confident assignments of glycerophospholipids at the sum composition (*e.g.*, phosphatidylcholine [PC] 34:1; with 34 fatty acyl carbon units and 1 site of unsaturation) and molecular lipid (*e.g.*, PC 16:0_18:1, detailing the composition of each fatty acyl chain) levels of description. However, these approaches do not yield insights into the location(s) of double bonds within these lipids and thus do not resolve possible regioisomers that differ only in their site(s) of unsaturation.[26, 27] This limitation arises from the preference of low energy (< 100 eV) collision-induced dissociation (CID) –the mainstay of contemporary MS/MS analysis– to drive charge-directed unimolecular dissociation at, or adjacent to, heteroatoms with little or no cleavage of carbon-carbon bonds.[28] While high-energy (> keV) and multi-stage (*i.e.*, MS^n) CID have been shown to drive some carbon-carbon bond cleavages in complex lipids,[29-31] the desired fragmentation remains poorly efficient relative to competing heteroatom cleavages rendering these techniques relatively insensitive to isomeric variations.[32]

To surmount these limitations, a number of alternative approaches have emerged targeting double bond positional assignment in complex lipids that can be broadly classified as (1) chemical derivatization of carbon-carbon double bonds prior to mass spectrometry in order to activate sites of unsaturation toward fragmentation upon CID,[33-35] and (2) alternative methods of ion activation to promote either (2a) cleavage of most carbon-carbon bonds where interruptions at sites of unsaturation can be identified,[36-39] or (2b) selective carbon-carbon bond cleavage at, or adjacent to, alkene positions.[34, 40-42] Amongst several solution-phase derivatization strategies, including epoxidation and more recently aziridination and Diels-Alder reactions,[43-46] the most widely adopted approach is the Paternò-Büchi reaction that involves a [2+2] cycloaddition between the double bond and an appropriate ketone or aldehyde (*e.g.*, acetone, benzophenone) under exposure to UV-light.[16, 47-50] Once the cyclic oxetane products are formed in solution they are ionized, mass-selected and subjected to CID yielding two diagnostic product ions with aldehyde and trisubstituted alkene motifs. The characteristic spacing between these two marker ions (Δm = 26.0520 Da when using acetone) in the resulting spectrum can be exploited for *de novo* assignment of the double bond position (**Scheme 1A**).[47] Although these approaches have been successful in assigning site(s) of unsaturation across a range of lipid classes, wet-chemical derivatization prior to mass spectrometry can significantly increase mixture complexity and requires more significant alteration to established lipidomics workflows.[34, 51] The alternative strategy is to interrogate the structure of unmodified lipid ions inside the mass spectrometer using auxiliary ion activation modalities to complement CID. The two most prominent of these tandem mass spectrometry methods have been ultraviolet photodissociation (UVPD)[52-59] and ozone-induced dissociation (OzID).[17, 60-68] Both techniques have been demonstrated to provide assignment of site(s) of unsaturation and the mass spectral resolution of regioisomers with successful integration into both direct infusion ("shotgun")[54, 66] and LC-MS/MS lipidomics protocols.[65, 69]

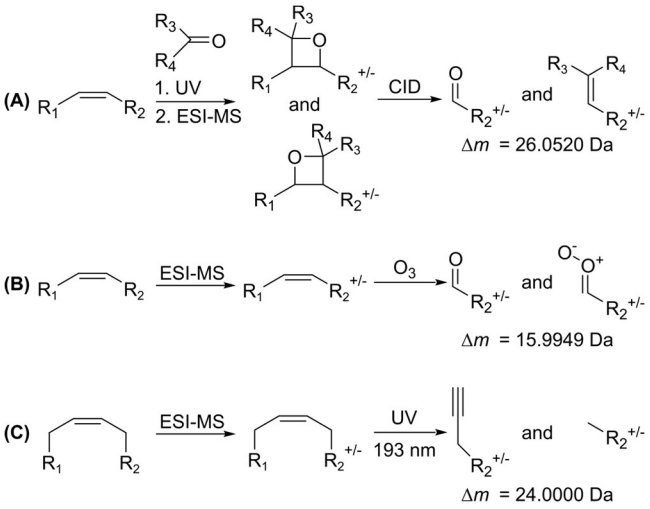

Scheme 1. Mass spectrometry techniques for analysis of double bond positions in lipids through either **(A)** Paternò-Büchi reaction with acetone ($R_{3/4}$ = CH_3) and subsequent CID, or ion activation by **(B)** ozone-induced dissociation or **(C)** UV-photodissociation to yield in all cases diagnostic product ions.

Ozone-induced dissociation exploits the gas-phase reaction of mass-selected lipid ions with ozone and has rapidly developed over the last decade with application to structural elucidation of a range of lipid species including fatty acids, glycerophospholipids and sterols.[60-62, 65, 70, 71] Pinpointing site(s) of unsaturation within fatty acyl chains is enabled through the selective chemically-induced cleavage of the double bond with product ions retaining either one or two oxygen atoms from the ozone. Known as the aldehyde and Criegee ions, the characteristic peak spacing of Δm = 15.9949 Da in an OzID spectrum provides for ready identification of the site(s) of unsaturation and resolution of any double bond regioisomers that may be present (**Scheme 1B**). Similarly, UVPD can be applied to the activation of ionized and mass-selected lipid ions to establish key features of their molecular structure, including double bond position(s) in unsaturated fatty acyl moieties.[52, 54, 57] UVPD of lipid ions at 193 nm or 213 nm has been found to be the most informative with absorption of these wavelengths promoting cleavage of allylic bonds and leading to putative alkyne and alkane product ions separated by Δm = 24.0000 Da, pinpointing the location of the double bond(s) (**Scheme 1C**).

The predictability of both OzID and UVPD fragmentation patterns have led to increased adoption of both technologies for lipid discovery and the automation of the requisite data analysis,[71-74] including the incorporation into existing software packages.[75] The combination of these factors has led to the observation and reporting of many hitherto undocumented lipids in previously well-studied reference materials. For example, some of us have recently used OzID technologies to document almost one hundred additional lipids present in NIST SRM 1950 reference human plasma.[71] In most such cases, no authentic reference lipids are available to validate structural assignments, placing greater emphasis on a complete understanding of the ion chemistries (including photochemistries) of OzID and UVPD to mitigate false positive assignments. Moreover, wherever possible, structural assignments for novel lipids should be based on multiple, orthogonal tech-

nologies,[76, 77] such as chromatographic or ion-mobility separation coupled with further structural elucidation techniques.[78, 79] To-date, however, limited examples exist where lipidomics analyses have been conducted across different platforms accessing multiple modes of ion activation. In response to this capability gap, we have implemented both OzID and UVPD on the same high-resolution mass spectrometry platform and undertaken parallel direct-infusion analysis in both modalities. Herein, we compare the information provided from mass spectra arising from parallel ion activation of reference standards, under directly comparable instrumental conditions, to explore the efficiency of each modality and to rigorously examine product ions that could potentially lead to false positive assignments of unsaturation location. These new mechanistic insights are used to inform analysis of unsaturated phosphatidylcholine lipid species within isogenic colorectal cancer cell lines, with both methods measuring consistent changes in relative abundances of *n*-7 to *n*-9 isomers of monounsaturated membrane lipids and revealing the presence of a non-canonical *n*-5 monounsaturated species.

EXPERIMENTAL

Lipid Nomenclature

The lipid structure nomenclature used here is based upon the LipidMAPS consortium recommendations,[80] modified to accommodate the *n-x* shorthand notation,[81] where *n* stands for the number of carbon atoms in the acyl chain and subtraction of *x* gives the position of the carbon-carbon double bond from the methyl terminus (*e.g.*, FA 18:3*n*-6,9,12 has an 18 carbon acyl chain with three carbon-carbon double bonds, the first of which is located at carbon 6 when counting from the methyl terminus). Where known, the geometry about the double bond is indicated as *cis* (*Z*) or *trans* (*E*). For PCs with known acyl chain orientation, the *sn*-1 is followed by the *sn*-2 acyl chain composition and separated by a forward slash (*e.g.*, PC 16:0/18:1*n*-9,*cis*), whilst acyl chain composition is separated by an underscore where the *sn*-position is not known or a mixture of both isomers is likely present (*e.g.*, PC 16:0_18:1*n*-9,*cis*) .

Materials

The following chemicals were obtained and used without further purification: *cis*-vaccenic acid (FA 18:1*n*-7,*cis*), oleic acid (FA 18:1*n*-9,*cis*), butylated hydroxytoluene (BHT), lithium acetate, and sodium acetate were purchased from Sigma-Aldrich. 1,2-Dioleoyl-glycero-3-phosphocholine (PC 18:1*n*-9,*cis*/18:1*n*-9,*cis*) was purchased from Avanti Polar Lipids. The structures and monoisotopic exact masses of all FA and PC standards included in the study are shown in **Table S1**. Complex whole cell lipid extracts from DLD1 parental colorectal cancer cells, which are heterozygous for mutant *KRAS*, or from DLD1 cell lines with knock-out of the *KRAS* wild-type (DLD1 KRAS:Mut) or mutant (DLD1 KRAS:WT) allele were obtained as described previously.[57] DLD1 MEK1 (-/-) and MEK2 (-/-), having double knockout mutation of *MEK1* and *MEK2* genes, respectively, were purchased from Horizon Discovery (Cambridge, UK). Methanol (CH_3OH) was purchased from Merck Millipore (Bayswater, VIC, Australia). Isopropyl alcohol (IPA) was purchased from Fisher Scientific (Hampton, NH, USA). Chloroform ($CHCl_3$) was purchased from Ajax Finechem (Taren Point, NSW, Australia). Eppendorf twin-tec 96-well PCR plates and Teflon Ultra-Thin Sealing Tape were purchased from Analytical Sales and Services (Flanders, NJ, USA).

Sample Preparation

Stock solutions of FA 18:1*n*-7,*cis*; FA 18:1*n*-9,*cis*, and PC 18:1*n*-9,*cis*/18:1*n*-9,*cis* were prepared in isopropanol with 0.01% (w/v) BHT, at concentrations of 10 mM. Working solutions were then prepared by placing 198 µL isopropanol:methanol:chloroform (4:2:1, v:v:v) containing 2 mM lithium acetate or sodium acetate into a vial, followed by addition of 2 µL of each individual stock solution, giving a final lipid concentration of 100 µM. For the cells, lipids extracted from *ca*. 2×10^7 pelleted cells of each cell line (as previously described) were re-suspended in 500 µL isopropanol/methanol/chloroform (4:2:1, v:v:v) 0.01% BHT. Working solutions were then prepared by diluting the cell extracts 50 times in isopropanol/methanol/chloroform (4:2:1, v:v:v) containing 2 mM lithium acetate.[57, 82, 83] 50 µL of each sample were then loaded into individual wells of an Eppendorf twin-tec 96-well PCR plate and sealed with Teflon Ultra-Thin Sealing Tape prior to MS analysis.

Instrumentation

All samples were analyzed using a Q Exactive Orbitrap mass spectrometer (Thermo Fisher Scientific, Bremen, Germany), interfaced with a robotic nano-electrospray ionization (nESI) source (TriVersa NanoMate, Advion, Ithaca, NY, USA) operating in positive ionization mode (spray voltage of 1.2 kV and gas pressure of 0.3 psi). The automated gain control (AGC) target of the Orbitrap mass analyzer was maintained at 1×10^6 and the maximum injection time was set to 500 ms. For MS/MS experiments, monoisotopic lipid ions were mass-selected using an isolation window of ±0.25 Da and data acquired at a mass resolving power of 70,000 (defined at *m/z* 200) over the *m/z* range 50 – 350 (FA standards), 100 – 1200 (PC standard), or 100 – 1000 (PCs from DLD1 cell lines). Higher-energy collision dissociation (HCD)-MS/MS spectra were generated with a HCD collision energy (CE) of 30 or 35 eV. The mass spectrometer was modified to provide both optical access and delivery of ozone to the HCD hexapole region (**Figure S1**). Modifications of this instrument to enable optical access and irradiation of isolated ions with a 193 nm Coherent Excistar XS ArF excimer laser system (Santa Clara, California, USA) have been previously described.[53] In brief, the laser light was directed coaxially, but slightly off-axis, into the HCD cell *via* a CaF_2 optical window introduced into the rear access port of the vacuum manifold with control of the number of laser shots and delay between shots within a given UVPD activation period achieved using a Berkeley Nucleonics Corporation (San Rafael, California, USA) model 505 pulse generator. For UVPD experiments, nitrogen was used as the collision gas and was supplied through the native system to yield an operating pressure of *ca*. $4 – 5 \times 10^{-5}$ mbar (HCD trap gas at 1.0 au). 193 nm UVPD-MS/MS spectra were obtained following introduction of mass-selected lipid ions into the HCD cell (CE = 2 eV, unless otherwise stated), using a 700 V discharge voltage (*ca*. 1 mJ laser energy) and irradiation times of 50 or 100 ms (~50 - 100 laser shots), prior to mass analysis.

Customization of Q Exactive geometry instruments for OzID have previously been undertaken in collaboration with Thermo Fisher Scientific.[66] Briefly, ozone (*ca.* 10-11% w/w in O_2) was produced online by a HC-30 ozone generator (Ozone Solutions, Hull, IA, USA) and catalytically destroyed in a closed-loop system operated with an oxygen flow of *ca*. 0.2 L

min^{-1}. A split flow from the closed loop was used as a supply for the mass spectrometer and introduced into the HCD cell *via* a PEEK restriction (127 μm × 2 m) delivering a pressure of *ca*. 4 – 5 × 10^{-5} mbar (HCD trap gas at 0.1 au, to mimic standard operation). This represents an estimated ozone number density of *ca*. 10^{13} molecules cm^{-3} based on the relative reactivity of the sodium adduct ion of trioleoylglycerol [TG 54:3+Na]$^+$ toward ozone compared to that observed previously on similar instrumentation.[65] For OzID, mass-selected lipid ions were injected into the HCD cell using a collision energy of 2 eV (except under combined collision- and ozone-induced dissociation conditions where CE = 30 eV) and then allowed to react with ozone for periods (defined by the activation time) of 10 – 1000 ms before mass analysis.

The experimental MS/MS variables described above resulted from optimization aimed at maximizing signal-to-noise for both ion activation modalities while maintaining approximately equal cycle times. Acquisitions in both modalities utilized one microscan per scan and the comparison between the techniques is based on analysis of spectra averaged over the same acquisition time (0.23 min for FA standards, 0.09 min for PC 36:2 standard, and 0.17 min for PCs from DLD1 cell lines).

Data Analysis

The raw mass spectra were inspected and scans averaged over the specified amount of acquisition time using Qual Browser within the native Xcalibur software (Version 3.0, Thermo Scientific, Bremen, Germany). Exact masses (4 d.p.), peak intensities and noise (calculated by Xcalibur as part of the flag data) for all ions in the spectrum list were then exported into a custom-built Microsoft Excel spreadsheet (Office 2016 program suite, Microsoft, Seattle USA) for further analysis. The spreadsheet is provided as Supporting Information and was constructed to automate analysis of the abundances of diagnostic ions for double bond position by each ion activation technique.

Briefly, the experimental precursor ion *m/z* (to 4 d.p.) is manually specified in the spreadsheet from which a list of theoretical diagnostic ion *m/z* for double bond or *sn*- position is generated based on the predicted neutral loss/gain from the activation technique (**Table S2** – **S5**). The theoretical ion *m/z* is then matched to the imported experimental data using the XLOOKUP function in Excel and a subset of experimental ions is generated that possess the smallest mass discrepancy from the theoretical ions. This list is then filtered by a mass tolerance threshold, Δ*m*, determined from a 5 ppm mass accuracy of the precursor ion (*i.e.*, ±0.0015 Da for FAs, and ± 0.0037 - 0.0041 Da for PCs), and a signal-to-noise (S/N) threshold (>3 for identification, >10 for quantification) that are input manually. For double bond isomers, the S/N was determined by dividing the ion abundance by the noise from the imported flag data for each diagnostic ion. For *sn*-isomers, the S/N was determined by dividing the sum of ion abundances by the sum of the noise from the imported flag data for the diagnostic ions. The normalized abundances of the filtered, diagnostic ions are then summed to obtain the abundance of the double bond isomer, further calculated relative to the most abundant double bond isomer, or the abundance of the *sn*-isomer.

RESULTS & DISCUSSION

Comparison of UVPD and OzID for fatty acid reference standards

For this study, UVPD (at 193 nm) and OzID were applied to equivalent, mass-selected ions trapped within the HCD cell of the Q Exactive with all other instrument conditions maintained to be as similar as possible. The two methods were initially compared with a variety of unsaturated lipid standards to explore the consistency and reliability of identification of the double bond position. Using the modified Q Exactive platform (*vide supra*), shotgun nESI of methanolic solutions of the two fatty acid (FA) 18:1 isomers, *cis*-vaccenic acid (FA 18:1*n*-7,*cis*) and oleic acid (FA 18:1*n*-9,*cis*), spiked with lithium acetate gave rise to abundant [M-H+2Li]$^+$ ions. Relative to other alkali metals, lithium adducts yield the highest relative abundance of diagnostic product ions under both UVPD and OzID activation modes.[57, 62]

OzID-MS/MS and UVPD-MS/MS of the [M-H+2Li]$^+$ precursor ion (*m/z* 295.3) formed from FA 18:1*n*-7,*cis* are shown in **Figure 1A** and **B**, respectively. In both spectra the diagnostic pairs of peaks arising from cleavage at (or adjacent to) the carbon-carbon double bond are readily identifiable and are consistent with predictions based on already established fragmentation rules for each modality (see neutral loss predictions in **Table S2** and **S3**).[57, 66, 84] Specifically, an abundant pair of OzID product ions at *m/z* 213.1645 ($C_{11}H_{19}O_3Li_2^+$) and *m/z* 229.1593 ($C_{11}H_{19}O_4Li_2^+$) are observed after only 10 ms of activation time (**Figure 1A**). The ions are separated by the mass of one oxygen atom (Δ*m* = 15.9949 Da) and may be assigned as the aldehyde and Criegee ions following decomposition of the primary ozonide (**Scheme 2A**);[61] noting the latter species may rearrange to a more stable carboxylic acid or a vinyl hydroperoxide.[60, 84, 85] Interestingly, a range of other abundant product ions are observed and can be assigned by accurate mass to neutral adducts of NO_2 and H_2O (**Figure 1A**). While some level of background water is unavoidable in most mass spectrometers, nitrogen oxides are a specific by-product of ozone generation and have previously been observed to cluster with some ion types under OzID conditions.[19] For comparison with OzID, 193 nm UVPD of the FA 18:1*n*-7,*cis* [M-H+2Li]$^+$ precursor ion on the same instrument yields the predicted pair of product ions at *m/z* 185.1695 ($C_{10}H_{19}O_2Li_2^+$) and *m/z* 209.1695 ($C_{12}H_{19}O_2Li_2^+$) separated by the mass of two carbon atoms (Δ*m* = 24.0000 Da, **Figure 1B**). These ions may be assigned as alkane and alkyne species, respectively, and have been proposed to be formed by a photo-initiated 1,2-elimination (**Scheme 2B**).[57] Whether this fragmentation occurs directly through an excited electronic state surface or from vibrational excitation on the ground state surface remains to be determined.[86] In addition to the diagnostic product ions, secondary neutral clustering reactions with water (+18 Da, UVPD and OzID) and nitrogen dioxide (+46 Da, OzID only) appear to be a feature of the dilithiated ions and their abundances were therefore taken into account when comparing the efficiency of each technique (**Figure 1**). Thus, under similar conditions, the yield of *n*-7 related product ions (*m/z* 213.2 and 229.2, 231.2 and 247.2, 259.2 and 275.2) is *ca*. 282% of the precursor ion (*m/z* 295.3 and 341.3) by OzID after only 10 ms, whilst the yield of product ions (*m/z* 185.2 and 209.2, 203.2 and 227.2) formed by UVPD is *ca*. 7% at a longer ion activation time of 50 ms. For dilithiated oleic acid, the diagnostic

pair of ions indicative of the carbon-carbon double bond at the *n*-9 position are also produced by OzID (*m/z* 185.1331 and *m/z* 201.1280 in **Figure 1C**, Δm = 15.9949 Da, corresponding to $C_9H_{15}O_3Li_2^+$ and $C_9H_{15}O_4Li_2^+$, respectively) at greater abundances despite a shorter activation time than UVPD (*m/z* 157.1384 and *m/z* 181.1382 in **Figure 1D**, Δm = 23.9998 Da, corresponding to $C_8H_{15}O_2Li_2^+$ and $C_{10}H_{15}O_2Li_2^+$, respectively) with the yield of *n*-9 related product ions at *ca*. 279% and 8%, respectively. Parallel analysis of an approximate 1:1 (w/w) mixture of the two isomeric fatty acids found diagnostic ions for each contributor across both modalities with no overlap of the diagnostic peaks as occurs with collisional activation of these ions (*cf*. **Figure S2** and **Figure S3**). The relative abundance ratios between the sum of isomer-specific signals in this mixture were found to be in reasonable agreement between the two orthogonal ion activation techniques with *n*-9:*n*-7 = 1.41 and 1.61 for OzID and UVPD, respectively.

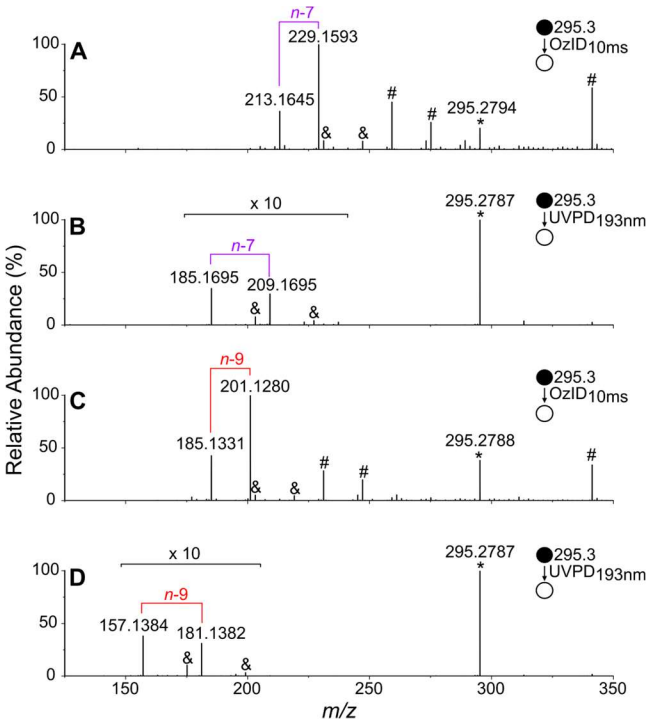

Figure 1. Tandem mass spectra of the $[M\text{-}H+2Li]^+$ adduct ions (indicated by *) formed by nESI of isomeric reference fatty acid standards (**A** and **B**) FA 18:1*n*-7,*cis* and (**C** and **D**) FA 18:1*n*-9,*cis* acquired on the modified Q Exactive mass spectrometer with ion activation by (**A** and **C**) OzID with a 10 ms reaction time or (**B** and **D**) UVPD at 193 nm with a 50 ms irradiation time. Product ions indicative of *n*-7 and *n*-9 are highlighted in color for both modalities with additional non-covalent adducts with neutrals NO_2 (#) and H_2O (&), as indicated.

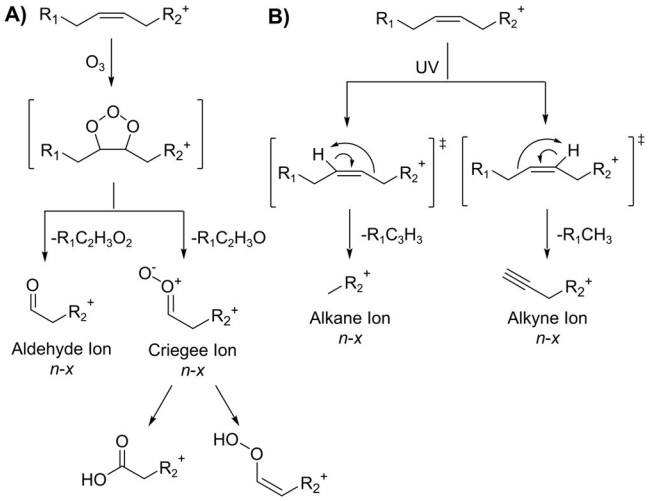

Scheme 2. Previously proposed mechanisms to account for the formation of product ions via bond cleavage at, or adjacent to, carbon-carbon double bonds induced by **A)** OzID[60] and **B)** UVPD.[57]

The spectral data from FA 18:1 reference standards (summarized in **Figure 1**) were further subjected to *de novo* analysis using OzID and UVPD neutral losses predicted for all theoretical double bond positions (*n*-1 to *n*-16) based on the neutral losses listed in **Table S2** and **S3**. Applying these rules using a S/N threshold of 10 (for quantification and 3-10 for detection) and a mass tolerance of ±0.0015 Da for both product ions (see methods section) recovers numerous putative double bond positions across both methods that are summarized in **Figure 2**. For FA 18:1*n*-7,*cis*, *de novo* analysis of the OzID data returned the expected *n*-7 double bond, based on the diagnostic Criegee and aldehyde ions already highlighted in **Figure 1A**. In addition, however, the analysis output putative double bond assignments from *n*-5 to *n*-13, albeit < 0.8% relative abundance compared to the sum of the *n*-7 signals (**Figure 2A**). Equivalent analysis for FA 18:1*n*-9,*cis* is summarized in **Figure 2C** with characteristic ions observed above S/N thresholds for positions from *n*-7 to *n*-13 by OzID, although these are < 0.3% relative abundance compared to the sum of the expected *n*-9 aldehyde and Criegee ions. The observation of OzID transitions outside those expected for the site of unsaturation in the reference fatty acids indicates one or more of the following: (i) the reference standards include trace amounts of alternate fatty acid isomers; (ii) ionization, mass-selection or ion ejection of the $[M\text{-}H+2Li]^+$ cations promotes some fragmentation or isomerization and/or; (iii) the ion activation modality itself promotes competing or secondary chemistries giving rise to false positives. Considering each of these in turn:

(i) The assignment of low abundant signals (0.73% of *n*-7 signal intensity) consistent with oleic acid (FA 18:1*n*-9,*cis*) in the FA 18:1*n*-7,*cis* OzID data (**Figure 2A**) are very likely the result of the former being a common background contaminant in ESI-MS,[87] with a recent study highlighting that a variety of background lipids from labware and solvent contamination may interfere with quantitation at very low concentrations.[88] Conversely, the considerably lower abundance of *n*-7 signals (only 0.14% of *n*-9 signal intensity, **Figure 2C**) in the reference data from FA 18:1*n*-9,*cis* suggests that cross contamination between samples was negligible and instead suggests that these signals result from ion chemistry within the mass spectrometer.

(ii) $[M-H+2Li]^+$ ions formed from fatty acids have previously been utilized to promote charge-remote fragmentation[89-92]; a process of unimolecular dissociation that cleaves carbon-carbon bonds and produces terminal alkene product ions that could potentially undergo reaction with ozone. To explore this possibility, CID of the ionized fatty acids was undertaken and shows that, while the terminal alkene product ions could be produced at low abundance, these required significantly higher collision energies compared to the HCD injection energies applied in either OzID or UVPD experiments (*i.e.*, 35 eV in **Figure S2** versus 2 eV in **Figure 1**). Moreover, the range and abundance of terminal alkene product ions did not match the assignments obtained from analysis of the OzID data (*i.e.*, *n*-9 to *n*-16 versus *n*-5 to *n*-14). While the threshold for charge-remote fragmentation may not be met under the OzID and UVPD conditions applied in the present study, charge-mediated isomerization of the double bond below the thresholds for dissociation may be possible. Indeed, Harvey has previously proposed charge-directed fragmentation pathways to account for dissociation of lithiated fatty acids involving an initial hydride transfer from the acyl chain to the electrophilic carbonyl carbon.[93] This charge migration may also provide a low energy pathway to double-bond migration *via* an allylic carbocation and thus unimolecular isomerization of the ionized fatty acid (see **Scheme S1**). Although low-energy unimolecular isomerization of this type has not previously been observed in cationized lipids containing fatty acyl moieties (*e.g.*, disodiated oleic acid,[61] monolithiated fatty acid methyl ester 18:2*n*-6,12,[62] or monolithiated cholestanyl oleate[70]), it is possible that the activation of the carboxylate moiety with two highly electrophilic lithium cations is able to promote the process in this special case. Even taking this into account, the degree of isomerization is low (with an upper limit of < 0.8%, **Figure 2**) and is only detectable due to the inordinately high reactivity of the $[M-H+2Li]^+$ ion type toward ozone.

(iii) The potential for false positive double bond position assignments in **Figure 2A** and **C** arising from competing or secondary ion-molecule reactions with ozone were also considered. As outlined in **Scheme 2**, the classical mechanism for alkene ozonolysis involves formation of either carboxylic acids and/or vinyl hydroperoxides following rearrangement of the Criegee intermediate. While the former is likely unreactive toward ozone, the vinyl hydroperoxide incorporates an activated, electron-rich olefin that may further react to give second generation aldehyde and Criegee ions,[94] that would be identical to the primary ozonolysis product ions of an *n*-(*x*+1) isomer (**Scheme 3A**). The secondary reaction of ozonolysis products could account for the observation of putative *n*-8 signals from the *n*-7 standard and *n*-10 signals from the *n*-9 standard. As illustrated in **Figure 2**, the abundance of these secondary product ions is significantly greater than the rest of the false positive signals with the exception of the *n*-9 signals observed in FA 18:1*n*-7,*cis* (**Figure 2A**) that likely have a contribution from background oleic acid (*vide supra*). The secondary reaction pathway proposed here for dilithiated fatty acid standards is consistent with previous observations from other lipid classes and ion types particularly at longer reaction times or higher ozone conentrations.[71] In previous studies, this has been corrected for by applying a threshold (1.5% for *cis* double bonds and 3.0% for *trans* double bonds) during data analysis to avoid false assignment of the double bond position, which the results in **Figure 2** suggest is a conservative threshold. Further over-oxidation to form *n*-(*x*+2) isomers is plausible for the highly reactive $[M-H+2Li]^+$ ions, but this would only account, for example, for a very small percentage of the observed *n*-11 isomer from FA 18:1*n*-9,*cis*.

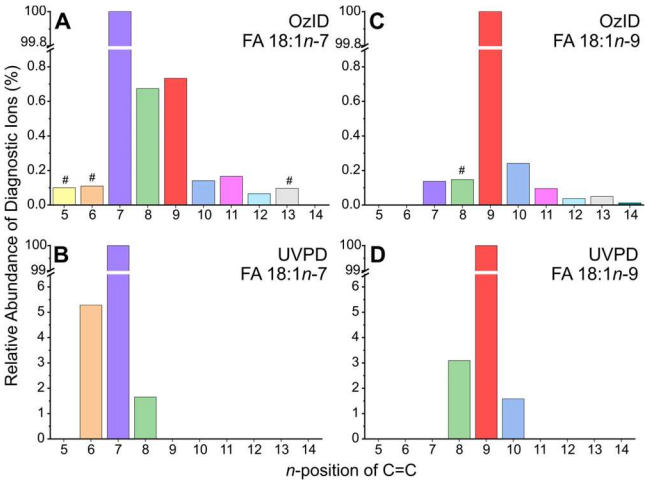

Figure 2. Relative abundances of the sum of diagnostic ions for putative double bond position in $[M-H+2Li]^+$ ions of *cis*-vaccenic acid by **(A)** OzID and **(B)** UVPD, and oleic acid by **(C)** OzID and **(D)** UVPD. Peaks marked # indicate that one of the diagnostic ions had 3 < S/N < 10. See **Table S6** for abundances relative to the signals corresponding to *n*-7 and *n*-9 double bond positions, respectively.

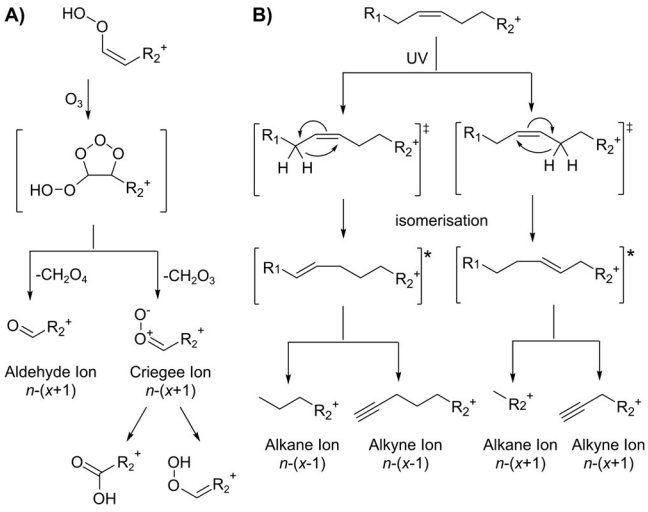

Scheme 3. Proposed mechanisms for formation of *n*-(*x*±1) product ions by **A)** secondary reaction of the vinyl hydroperoxide with ozone in OzID and **B)** competing sigmatropic 1,3-hydrogen atom shifts leading to isomerization prior to dissociation in UVPD.

The same *de novo* approach was applied to analysis of the UVPD mass spectra of the $[M-H+2Li]^+$ ions from FA 18:1*n*-7,*cis* and FA 18:1*n*-9,*cis* reference standards. The results are summarized in **Figure 2B** and **D**, respectively. Applying the UVPD neutral loss predictions from **Table S3** and the same signal-assessment criteria as used for OzID returned fewer putative assignments. The native *n*-7 double bond in *cis*-vaccenic acid was detected as the major isomer by UVPD (highlighted in **Figure 1B**), but with significant abundance in signals identified as putative *n*-6 (*m/z* 199.1852 $C_{11}H_{21}O_2Li_2^+$ and *m/z* 223.1851 $C_{13}H_{21}O_2Li_2^+$, 5.2% of *n*-7 signal intensity) and *n*-8 (*m/z* 171.1540 $C_9H_{17}O_2Li_2^+$ and *m/z* 195.1540 $C_{11}H_{17}O_2Li_2^+$, 1.8% of *n*-7 signal intensity) double bonds (**Figure 2B**). A similar trend was observed for oleic acid with analysis of UVPD spectra detecting the *n*-9 double bond as the

major signal but bracketed by significant signals consistent with *n*-8 (3.2%) and *n*-10 (1.6%) double bond positions (**Figure 2D**). The presence of these additional signals that are consistent with neutral loss predictions from UVPD requires consideration of the same three possible explanations as for the OzID data (*vide supra*):

(i) The absence of detectable *n*-6 signals in the spectra from FA 18:1*n*-9,*cis* and conversely the absence of *n*-10 signals in the spectra from FA 18:1*n*-7,*cis* rule out a consistent background source of the corresponding fatty acid isomers as the source of these signals. Moreover, there is no signal of equivalent relative abundance in the OzID analysis despite the demonstrated higher sensitivity of the latter method for this system. The disparate sensitivities for this ion type might also explain why no *n*-9 signals are detected in the UVPD shown in **Figure 2B** despite an apparent contribution of background oleic acid in the OzID data obtained from FA 18:1*n*-7,*cis*. However, doubling the number of laser shots from 50 to 100 for the FA 18:1*n*-7,*cis* standard afforded increased signal-to-noise in some low abundant product ions consistent with the *n*-9 and *n*-13 assignments made by OzID (**Figure S4A**).

(ii) When data are obtained under comparable conditions, the UVPD analysis does not reveal the myriad of ions observed from OzID (*cf*. **Figure 2A** and **C** with **Figure 2B** and **D**, respectively). Again, doubling the number of laser shots from 50 to 100 for the FA 18:1*n*-9,*cis* standard increased the abundance of product ions consistent with the *n*-7 to *n*-12 assignments made by OzID and providing further evidence for isomerization of a very small population of the $[M\text{-}H+2Li]^+$ species during ionization or transmission (**Figure S4B**). This process, however, cannot account for the abundant *n*-(*x*±1) (where *x* = 7 or 9, respectively) that are associated with the UVPD analysis.

(iii) With the pairwise comparisons between fatty acid isomers and between ion activation modalities effectively ruling out sample contamination or isomerization of the ions as major contributors to the *n*-(*x*±1) signals in the UVPD-MS/MS spectra, competing photodissociation pathways need to be considered. The presence of one of the diagnostic ions from *n*-(*x*±1) in UVPD spectra of unsaturated lipids has previously been reported and rationalized as arising from competing photoisomerization processes, invoking a 1,5-hydrogen shift to produce the *n*-(*x*±1) alkane ion and an observed conjugated diene (**Scheme S2**).[57] In order to form the *n*-(*x*±1) alkyne ion, however, the conjugated diene would need to lose ethene that would likely require surmounting high potential energy barriers whilst competing with other, lower energy pathways.[95] An alternative proposal could explain the *n*-(*x*±1) product ions via initial sigmatropic 1,3-hydrogen atom shifts from each of the allylic positions (**Scheme 3B**).[86] From there, the canonical fragmentation mechanism in **Scheme 2** may be invoked to form the diagnostic alkane and alkyne species, though the differing relative amounts of the *n*-(*x*+1) to the *n*-(*x*-1) isomer suggests other interactions and mechanisms may be at play. Indeed, it is difficult to ascertain whether formation of these confounding product ions is directly competitive with the diagnostic marker ions or whether they are secondary products. In either case, careful assessment of UVPD data is required where *n*-(*x*±1) product ions are observed in the presence of abundant *n*-*x* isomers.

Taken together, the assessment of UVPD- and OzID-MS/MS spectra obtained under the same conditions for $[M\text{-}H+2Li]^+$ cations of monounsaturated fatty acids suggests that this ion type can promote a limited amount of unimolecular isomerization during ion formation or transfer that is independent of the ion activation modality. Whilst this a significant new mechanistic insight, it is unlikely to result in widespread false positive assignment of novel lipids in shotgun lipidomics as dilithiated cations are not widely deployed for fatty acid analysis. Of greater importance is the demonstration that under comparable conditions each ion activation modality generates product ions consistent with sites of unsaturation at the *n*-(*x*+1) position while, in addition, UVPD generates signals for an *n*-(*x*-1) double bond. Thus, the competing ion chemistries for the two orthogonal ion activation approaches prompted further comparison in other lipids.

Comparison of UVPD and OzID for phospholipid reference standards

To evaluate the ion activation behavior for complex lipids, PC 18:1*n*-9,*cis*/18:1*n*-9,*cis* was used to compare the two methods on the same instrument. The $[M+Li]^+$ ion at *m/z* 792.6 was mass-selected in an MS/MS experiment. The OzID spectrum obtained using a 100 ms reaction time is presented in **Figure 3A** and shows major product ion peaks at *m/z* 682.4614 ($C_{35}H_{66}NO_9PLi^+$) and *m/z* 698.4564 ($C_{35}H_{66}NO_{10}PLi^+$, Δm = 15.9950 Da) following ozonolysis of either *n*-9 double bond. The product ion abundances were much lower than those observed for the dilithiated fatty acids (*cf*. 2% versus 370% of the *n*-9 containing precursor ion), suggesting that the carbon-carbon double bond is less activated towards oxidation – most likely due to other polar moieties in the more complex structure coordinating the lithium cation and suppressing interactions with the double bond. As a result, a ten-fold longer reaction time was used here to compensate for the lower reactivity and maintain sufficient signal-to-noise of the product ions. Integrating the UVPD acquisitions for the same PC 36:2 $[M+Li]^+$ ions over a comparable time to the OzID experiment yields the spectrum shown in **Figure 3B**. The double bond-diagnostic ions are observed at *m/z* 654.4663 and *m/z* 678.4664 (Δm = 24.0001 Da) corresponding to $C_{34}H_{66}NO_8PLi^+$ and $C_{36}H_{66}NO_8PLi^+$, respectively, identifying the *n*-9 double bond in PC 18:1*n*-9,*cis*/18:1*n*-9,*cis*. In contrast to the dilithiated fatty acids, for the unsaturated phosphatidylcholines the conversion of precursor to product ions is comparable between OzID (2.3%) and UVPD (2.7%) approaches (**Table 1**). Furthermore, though ozone shows a large difference in reactivity towards the different standards as discussed, 193 nm photodissociation shows only slightly greater product ion abundances for the $[FA\text{-}H+2Li]^+$ ions (*cis*-vaccenic acid: 6.3%; oleic acid: 6.9%) compared to the $[PC+Li]^+$ ions (2.7%), suggesting that the latter technique is less sensitive to the nature of the lipid.

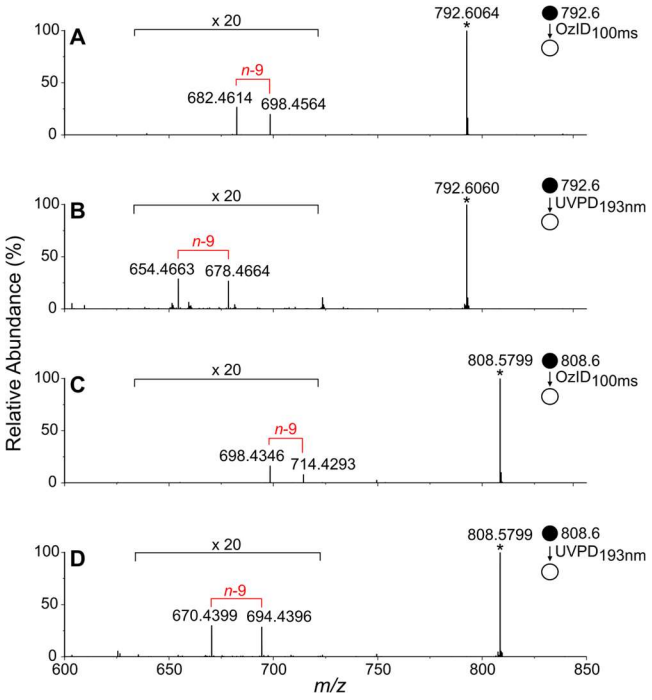

Figure 3. Tandem mass spectra of the $[M+Li]^+$ (**A** and **B**) and $[M+Na]^+$ (**C** and **D**) adduct ions (indicated by *) formed by nESI of reference phosphatidylcholine PC 18:1*n*-9,*cis*/18:1*n*-9,*cis* acquired on the modified Q Exactive mass spectrometer with ion activation by (**A** and **C**) OzID with a 100 ms reaction time or (**B** and **D**) UVPD with a 50 ms irradiation time. Product ions indicative of *n*-9 are highlighted in color for both modalities.

Table 1. Abundances of the sum of diagnostic ions for double bond position (*n*-*x*) in lithiated and sodiated PC 36:2 detected by OzID (at reaction times of 100 and 1000 ms) and UVPD (at irradiation times of 50 ms) as a percentage of the precursor ion abundance (as a percentage of the sum of *n*-9 diagnostic ions) for each modality.

	$[M+Li]^+$			$[M+Na]^+$		
n-*x*	OzID 100 ms	OzID 1000 ms	UVPD 50 ms	OzID 100 ms	OzID 1000 ms	UVPD 50 ms
n-8			0.08 (2.89)			0.10 (3.34)
n-9	2.33	19.7	2.73	1.18	10.9	2.89
n-10		0.14 (0.70)	0.05 (1.99)		0.09 (0.80)	0.07 (2.45)

To evaluate how the cation affects the two techniques when analyzing phosphatidylcholines, monosodiated PC 36:2 was also examined and fragment ions supporting an *n*-9 double bond were observed by both techniques (OzID: *m/z* 698.4346 and *m/z* 714.4293, Δm = 15.9947 Da in **Figure 3C**; UVPD: *m/z* 670.4399 and *m/z* 694.4396, Δm = 23.9997 Da in **Figure 3D**). OzID product ion yields for the sodiated cation are approximately half of the equivalent product ions from the $[M+Li]^+$ ion (sum of aldehyde and Criegee ion abundances 1.2% versus 2.3%), consistent with the previously observed lower reactivity of ozonolysis for $[M+Na]^+$ lipid ions (**Table 1**).[62, 70] In contrast, UVPD of the sodiated PC 36:2 yields a similar product ion abundance (2.9% of the precursor ion) to the lithiated ion (2.7%), reinforcing the notion that this technique is not as sensitive to the nature of the group 1 cation.[57]

De novo analysis using the same threshold criteria applied previously was undertaken for UVPD- and OzID-MS/MS spectra from PC 36:2 across both $[M+Li]^+$ and $[M+Na]^+$ ion types. Despite containing multiple oleic fatty acyl moieties equivalent to that used in the free fatty acid analysis (*vide supra*), OzID at 100 ms on both the $[M+Li]^+$ and $[M+Na]^+$ ions returned only the expected *n*-9 double bond (**Table 1**) with no evidence for the confounding product ions observed for FA 18:1 $[M-H+2Li]^+$ ions (*cf.* **Figure 2B**). However, increasing the OzID reaction time by ten-fold (to 1000 ms) enabled observation of product ions consistent with the *n*-10 double bond position with peak intensities *ca*. 0.7 and 0.8% of the *n*-9 signals for lithium and sodium, respectively. The presence of this *n*-(*x*+1) artifact can be rationalized as a secondary ozonolysis reaction of the initially formed vinyl hydroperoxide ion as previously discussed (**Scheme 3A**). The absence of other signals that would meet the criteria for double bond assignment in OzID indicates that the unimolecular double-bond migration observed for the $[FA-H+2Li]^+$ ions is not a feature of the phosphatidylcholine ion chemistry. Indeed, this result suggests that such isomerization (**Scheme S1**) is a characteristic of the highly electrophilic dilithiated carboxylic acid moiety and is unlikely to be a feature of complex lipids ionized in the modalities typically used in lipidomics.

Results from *de novo* analysis of the UVPD spectra acquired from lithiated and sodiated PC 36:2 are summarized in **Table 1**. In addition to the expected signals from unsaturation at the *n*-9 position, ions consistent with *n*-8 and *n*-10 are observed at ~3% and ~2%, respectively, of the *n*-9 signal (**Table 1**). Identification of these *n*-(*x*±1) artifacts in the UVPD spectra of PC 18:1*n*-9,*cis*/18:1*n*-9,*cis* is consistent with the observations for dilithiated FA 18:1*n*-9,*cis* with similar relative abundance of product ions (*cf.* **Figure 2D**). The phosphatidylcholine results thus support the origins of these artifacts as competing photoinduced isomerization or fragmentation pathways such as the proposal in **Scheme 3B**. Another similarity with the oleic acid model system is that the sum of the *n*-(*x*-1) ion abundance for PC 36:2 is greater than for the *n*-(*x*+1) ions, suggesting a potential pattern, or criterion, for inclusion or exclusion of potentially novel lipid isomers in the shotgun analysis of biological lipid extracts.

In addition to the double bond marker ions, close inspection of the UVPD-MS/MS spectra acquired under these experimental conditions revealed product ions also common to CID of metalated PC cations. For example, 193 nm activation of the $[M+Li]^+$ ions of PC 36:2 (*m/z* 792.6060, $C_{44}H_{84}NO_8PLi^+$) gave low abundant signals at *m/z* 733.5328 ($C_{41}H_{74}O_8PLi^+$), *m/z* 609.5414 ($C_{39}H_{70}O_4Li^+$) and *m/z* 603.5331 ($C_{39}H_{71}O_4^+$) corresponding to neutral losses of trimethylamine and phosphocholine (with and without retention of lithium, respectively), which are characteristic of the PC subclass (**Figure S5A**).[96, 97] In addition, ions at *m/z* 504.3434 ($C_{26}H_{51}NO_6P^+$) and *m/z* 510.3516 ($C_{26}H_{50}NO_6PLi^+$) are consistent with neutral loss of one of the 18:1 fatty acyl chains. Taken together for an unknown lipid, this single spectrum provides evidence for assignment of the lipid molecular structure beyond the site(s) of unsaturation alone. In contrast, closer inspection of the OzID data acquired under comparable conditions yields very low abundant product ions in these CID-like product channels (**Figure S5B**). However, increasing the collision energy to 35 eV for injection of the ions into the HCD cell in the presence

of ozone was found to yield a composite collision-/ozone-induced dissociation mass spectrum with many of the same product ions indicative of headgroup and acyl chain composition as observed under UVPD conditions (**Figure S5C**). Furthermore, these conditions also promote ozonolysis of CID product ions. For example, the product ions at *m/z* 389.2862 ($C_{22}H_{38}O_5Li^+$) and *m/z* 405.2810 ($C_{22}H_{38}O_6Li^+$, Δm = 15.9948 Da) in **Figure S5C** arise from the *m/z* 609.5404 ($C_{39}H_{70}O_4Li^+$) CID product ion and, as previously demonstrated, are indicative of an 18:1 acyl chain at the *sn*-1 position of the glycerol backbone.[63, 98] Analogous *sn*-specific second-generation product ions are also observed in the UVPD spectrum (**Figure S5A**),[54] indicating that spectra obtained by both modalities may be able to reveal the prevailing *sn*-isomer within a mixture. However, in the absence of re-isolation of the intermediate ion (*i.e.*, an MS^3 sequence) on the Q Exactive platform,[17, 54, 74] the relative abundance of these ions may not faithfully reproduce *sn*-isomer contributions. Nevertheless, both UVPD and OzID (with elevated CE) yield composite spectra that extend the structure elucidation of glycerophospholipids beyond assignment of double bond position.

Application of orthogonal UVPD and OzID ion activation for lipid structural assignment

Using lipid standards, we have established key heuristics that can improve the interpretation of UVPD and OzID mass spectra. Here, these orthogonal ion activation techniques are applied to a series of isogenic DLD1 colorectal cancer (CRC) cells to enable confident structural assignment of monounsaturated phosphatidylcholines.[99-102] Total lipid extracts from isogenic DLD1 CRC lines were analyzed *via* nESI in the presence of lithium acetate with mass-selected, unsaturated phosphatidylcholines subjected to alternating ion activation by OzID and UVPD. Representative mass spectra for the abundant monounsaturated lipids PC 32:1 and PC 34:1 from the DLD1 parental CRC cell line are presented in **Figure 4**. *De novo* analysis of these spectra using the double bond specific neutral losses for each technique (*i.e.*, **Table S2** and **S3**) for PC 32:1 identify abundant product ions corresponding to *n*-7 (OzID **Figure 4A**: *m/z* 656.4462 and 672.4408; UVPD **Figure 4B**: *m/z* 628.4510 and 652.4508) and *n*-9 double bond positions (OzID **Figure 4A**: *m/z* 628.4147 and 644.4100; UVPD **Figure 4B**: *m/z* 600.4204 and 624.4198). The observation of abundant signals for these two isomers by both techniques is confirmatory and consistent with canonical human lipid metabolism and prior measurements.[22] Notably, the processes leading to false positives from each technique following the *n*-(*x*+1) and *n*-(*x*±1) rules established above exclude contributions to the *n*-9 signals from *n*-7 (or vice versa). For both techniques, the product ions assigned to the *n*-7 are more abundant than those of the *n*-9 isomer with product ion ratios found to be comparable with the *n*-9 to *n*-7 ratio equal to 0.156 ± 0.002 and 0.204 ± 0.009 for OzID and UVPD, respectively (**Figure 5A**). Further, the major molecular lipid constituting PC 32:1 was determined by both CID-OzID and UVPD to be PC 16:0_16:1 with minor contributions of PC 14:0_18:1 (see **Table S7** and **Figure S6**). Isomeric phosphatidylethanolamines (*e.g.*, PE 16:0_19:1) were discounted based on the absence of the signal corresponding to loss of the PE headgroup in the HCD spectrum, *i.e.*, -141.0191 Da. Thus, despite the discussed differences between the two techniques, these independent ion activation methods both suggest that PC 16:0_16:1*n*-7 is present in greater abundance than PC 16:0_16:1*n*-9.

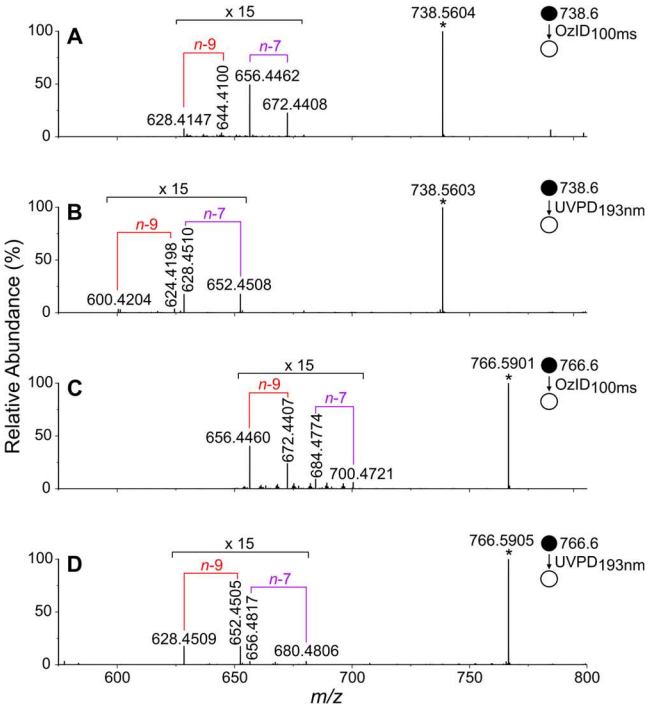

Figure 4. Tandem mass spectra obtained from the $[M+Li]^+$ adduct ions (indicated by *) formed by nESI of PC 32:1 (**A** and **B**) and PC 34:1 (**C** and **D**) from total lipid extracts of the parental DLD1 colorectal cancer cell line acquired on the modified Q Exactive mass spectrometer with ion activation by (**A** and **C**) OzID with a 100 ms reaction time or (**B** and **D**) UVPD with 50 ms irradiation time. Product ions indicative of *n*-7 and *n*-9 are highlighted in color for both modalities.

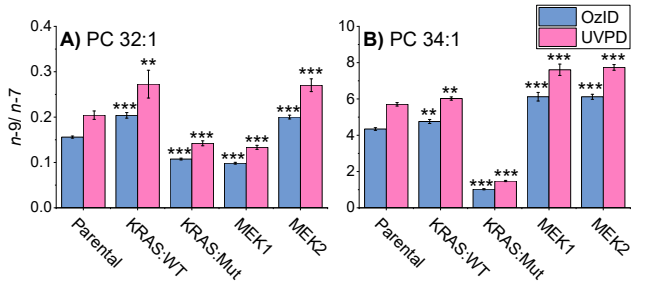

Figure 5. Ratios of *n*-9 to *n*-7 double bond isomers in **A)** PC 32:1 and **B)** PC 34:1 as detected by OzID and UVPD in DLD1 isogenic colorectal cancer cell lines. Statistical significance in changes in the *n*-9 to *n*-7 ratio between the parental cell line and each isogenic cell line (n = 3 technical replicates, except for KRAS:WT where n = 2) were evaluated for each technique using the 2-tailed Student's *t* test (*$P < 0.05$, **$P < 0.01$, ***$P < 0.001$).

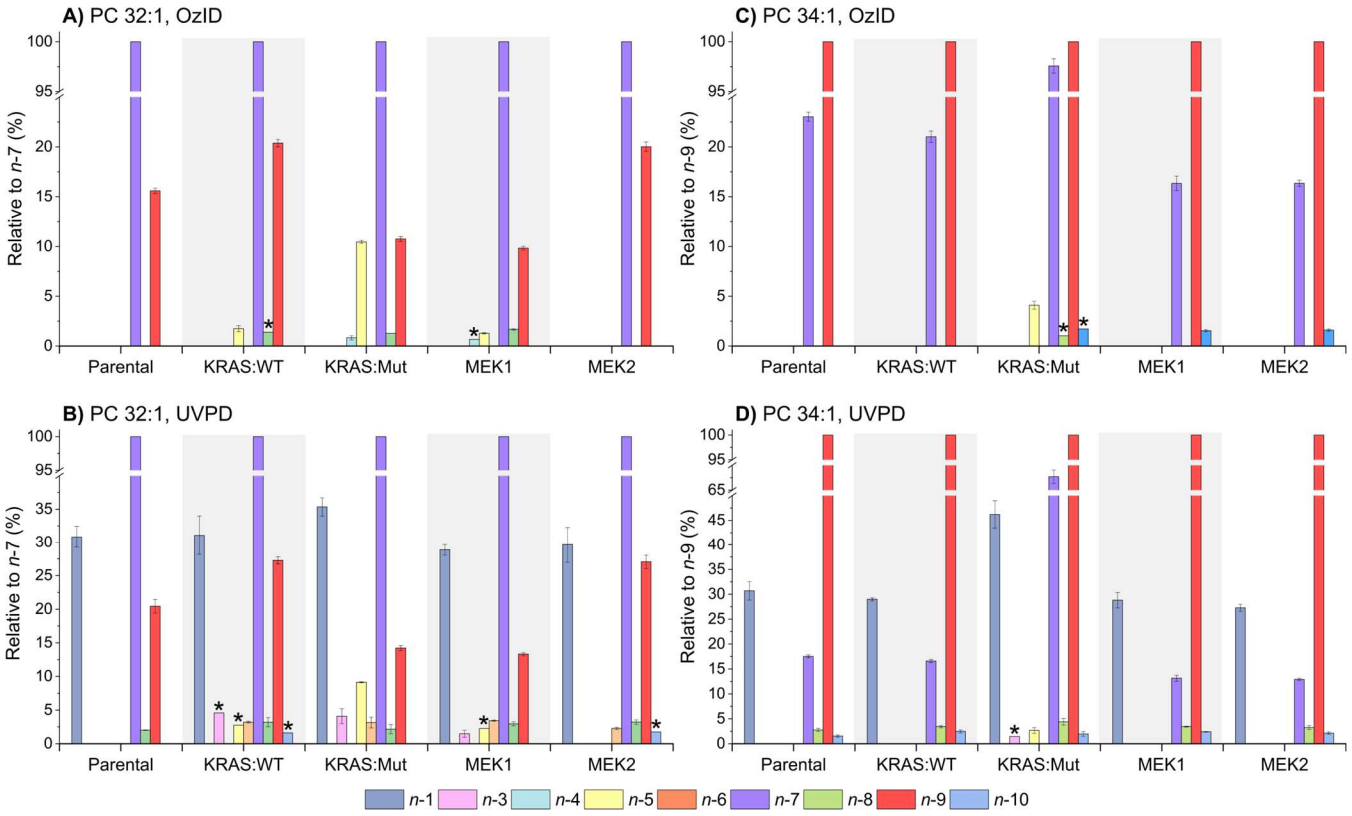

Figure 6. Relative abundances of the sum of diagnostic ions (S/N > 3) for putative double bond position in $[M+Li]^+$ ions of PC 32:1 (relative to *n*-7) by **(A)** OzID compared to **(B)** UVPD, and of PC 34:1 (relative to *n*-9) by **(C)** OzID compared to **(D)** UVPD from isogenic DLD1 colorectal cancer cell lines (n = 2 for KRAS:WT, n = 3 for others). * indicates that the double position was detected in only one technical replicate. See **Figure S8** for normalized abundances.

DLD1 parental CRC cells harbor an oncogenic mutation in *KRAS* (one mutant and wild-type *KRAS* allele). Extending the analysis of PC 32:1 to the DLD1 isogenic cell lines, where either the mutant or wild-type *KRAS* alleles have been disrupted (*i.e.*, DLD1 KRAS:WT and DLD1 KRAS:Mut, respectively),[82] the relative abundance of PC 16:0_16:1 was consistent across all cell lines (in addition to minor 14:0_18:1, trace PC 14:1_18:0 was also detected by CID-OzID, see **Table S7**). However, the fold change in the ratio of PC 16:0_16:1*n*-9 to PC 16:0_16:1*n*-7 by both techniques was consistent with an increase in the KRAS:WT by *ca*. 32% and a decrease in the KRAS:Mut cell lines by *ca*. 30% compared to the parental cell line (**Figure 5A** and **Table S8**). KRAS is a principal mediator of MAPK (MEK)/ERK signaling, and two additional isogenic DLD1 cell lines comprising knockouts of the downstream signaling kinases MEK1 and MEK2 were also examined to provide further insights into the role of MAPK/ERK signalling.[103] Compared to the parental DLD cells, MEK1 and MEK2 knockout showed opposite effects on the PC 32:1 *n*-9 to *n*-7 ratios with a reduction in the former by *ca*. 36% and increase in the latter isogenic line by *ca*. 30%, suggesting that the impact of mutant KRAS on *n*-9 to *n*-7 double bond isomers of palmitoleic acid-containing phosphatidylcholines may be mediated by MEK2 homodimers.

In addition to the major *n*-7 and *n*-9 isomers identified for PC 32:1, **Figure 6** summarizes the *de novo* analysis of the OzID spectra and UVPD mass spectra, which located a number of signals consistent with double bonds at the *n*-4, *n*-5 and *n*-8 positions (OzID) and *n*-1, *n*-3, *n*-5, *n*-6, *n*-8 and *n*-10 positions (UVPD). While the intensity of most of these signals is low compared to the diagnostic *n*-7 and *n*-9 product ions, they nonetheless meet the criteria for both mass accuracy and signal-to-noise (>3). Identification of signals corresponding to the *n*-5 double bond position in both OzID and UVPD, which cannot be an artifact of the *n*-(*x*±1) relationship from either of the abundant PC 32:1*n*-7 or PC 32:1*n*-9 product ions, confirms the presence of a PC 32:1*n*-5 isomer in several of the cell lines. The contribution of this isomer to the PC 32:1 population was *ca*. 10% for the KRAS:Mut cell line compared to 0 – 2% for the other isogenic cell lines (relative to the most abundant PC 32:1*n*-7, **Figure 6A** and **B**; see **Figure S7** for mass spectra), indicating a significant deviation in the desaturation metabolism for the KRAS:Mut cell line (significant uptake of FA 14:1*n*-5 into the PC 32:1 pool can be ruled out based on the molecular lipid analysis, **Table S7**).

Leveraging the orthogonal nature of the two ion activation modalities means that the presence of PC 32:1 isomers containing an *n*-1, *n*-3, *n*-6, or *n*-10 double bond based on the UVPD signals can be excluded due to the absence of corresponding signals by OzID (**Figure 6**). While the presence of these *n*-6 and *n*-10 ions in the UVPD analysis can be rationalized by the competing photodissociation pathways from the major PC 32:1*n*-7 and PC 32:1*n*-9 isomers (*i.e.*, an *n*-(*x*-1) and *n*-(*x*+1) false positive, respectively, *vide supra*), the sources of the putative *n*-1 and *n*-3 product ions warrant further discussion. The *de novo* analysis conducted here did not contain any thresholds for the relative abundance of the diagnostic ions to each other (*i.e.*, ratio of aldehyde to Criegee ions for OzID, or alkane to alkyne ions for UVPD) as previous studies using both ion activation techniques have shown variability in this parameter.[57, 78] Consequently, a very abundant ion generated by an alternative pathway may mask a minor ion that just

meets the signal-to-noise threshold for detection. The "alkyne" ion that corresponds to an *n*-1 signal in UVPD is formally produced by the loss of H_2, but this is not possible by the mechanism suggested in **Scheme 2**. Instead, this ion is more likely due to the energy supplied by the laser promoting a 1,4-elimination of H_2 about the double bond, previously detected upon collision-induced dissociation of monounsaturated fatty acids (**Scheme S4**).[28] In comparison, the variable abundance of the *n*-3 signals across the cell lines are suggestive of some biological source and as such are most likely the product of photodissociation of a minor, isobaric ion that is unreactive toward ozone. Similarly, the minor *n*-4 double bond detected by OzID in **Figure 6A** is not detected by UVPD and is hence likely to be an isobaric ion. Finally, the *n*-8 signals are not readily excluded by cross-validation as they are common to both techniques, however, they are *ca.* 1.2-1.6% by OzID and *ca*. 2.0-3.2% by UVPD of the *n*-7 peaks. This is in line with the threshold for *n*-(*x*+1) signals associated with PC 32:1*n*-7 overoxidation in the former, and the slightly higher thresholds in the latter for the overlapping *n*-(*x*+1) signals from photoisomerization of PC 32:1*n*-7 and *n*-(*x*-1) signals from photoisomerization of PC 32:1*n*-9.

For the $[M+Li]^+$ adduct of PC 34:1, *de novo* analysis of the mass spectra indicates the major isomer contains a double bond at the *n*-9 position by both ozonolysis (*m/z* 656.4460 and *m/z* 672.4407, **Figure 4C**) and photodissociation (*m/z* 628.4509 and *m/z* 652.4505, **Figure 4D**). By comparison, the *n*-7 isomer is only a minor contributor (OzID: *m/z* 684.4774 and *m/z* 700.4721; UVPD: *m/z* 656.4817 and *m/z* 680.4806). The *n*-9 to *n*-7 ratio in the DLD1 parental cell line is 4.34 ± 0.07 by OzID and 5.70 ± 0.18 by UVPD (**Figure 5B**), which shows the same bias as in PC32:1 with either OzID overestimating the relative abundance of *n*-7 or UVPD overestimating the relative abundance of *n*-9 and would require calibration to external standards to correct. Analysis at the molecular lipid level shows that PC 34:1 is comprised mostly of PC 16:0_18:1 across all cell lines with a minor amount of PC 16:1_18:0 (trace PC 14:0_20:1 and PC 14:1_20:0 were only detected by CID-OzID, see **Table S7**). In contrast to the major PC 32:1 double bond isomers, the changes in relative abundance of PC 16:0_18:1*n*-9 to PC 16:0_18:1*n*-7 across the cell lines show a smaller increase between the parental and KRAS:WT cells of *ca*. 8% and a larger reduction between the parental and KRAS mutant cells of *ca*. 75% by both techniques (**Figure 5B** and **Table S8**). Compared to the parental cell line, both the MEK1 and MEK2 knock-out resulted in an increase in the *n*-9 to *n*-7 ratio of *ca*. 37%, implicating both as potential mediators of the effect of mutant KRAS on octadecenoic acid-containing phosphatidylcholines. In addition to the minor PC 34:1*n*-5 detected by both techniques in the KRAS mutant cells, other double bond signals were also observed by both OzID (*n*-8 and *n*-10, **Figure 6C**) and UVPD (*n*-1, *n*-3, *n*-8 and *n*-10, **Figure 6D**). Following the rules established to identify false positives by OzID, the minor *n*-10 isomer may be explained as an overoxidation product of the major PC 16:0_18:1*n*-9 species. Similarly, the *n*-8 isomer is only observed in the mutant cell line by OzID as there is sufficient PC 16:0_18:1*n*-7 present for the *n*-(*x*+1) false positive signals to be above the signal-to-noise threshold. For UVPD, the putative *n*-8 and *n*-10 species may be rationalized as the *n*-(*x*±1) products from photoisomerization of the major *n*-9 isomer. The remaining UVPD signals may be discounted by cross-validation with OzID, noting the large abundance of *n*-1 is due to the charge-remote elimination of H_2 as discussed for PC 32:1, whilst the *n*-3 artifact is likely due to an isobaric species that is only reactive towards UV and not ozone.

In 30-50% of CRCs, activating mutations are present in the gene that encodes oncogenic KRAS, which modulates fatty acid synthesis enzymes such as fatty acid synthase (FASN), stearoyl-CoA desaturase-1 (SCD-1), and fatty acid elongase (ELOVL) *via* the atypical serine/threonine kinase mTOR protein that regulates cell growth and metabolism.[15, 104, 105] These changes in the double bond isomeric constitution of the two phosphatidylcholines across the isogenic CRC cell lines examined here suggest effects on the underlying biochemical pathways that synthesize/modify these lipids. Compared to the other cell lines, there is a significantly lower *n*-9 isomer population in PC 16:0_18:1 in the KRAS mutant cell line with a concomitant increase in the non-canonical *n*-7 isomer, potentially due to SCD-1 desaturation of the FA 16:0 component to FA 16:1 out-competing fatty acid elongation to FA 18:0 prior to incorporation into the more complex PC. This suggests downstream effects from KRAS mutation on desaturation and elongation enzymes such as SCD-1 and ELOVL6,[15, 22] with analysis of MEK1 and MEK2 isogenic cells suggesting potential mediation *via* either both kinases or MEK2 homodimers depending on the fatty acyl chain length. Similarly, the formation of an *n*-5 isomer in the mutant cell line would indicate that the precursor fatty acid 14:0 is being desaturated to FA 14:1*n*-5 preferentially to elongation to FA 16:0 due to increased expression or activity of SCD-1 (**Scheme S5**). This fatty acid is then elongated to FA 16:1*n*-5 and FA 18:1*n*-5, which are likely incorporated into PC 32:1*n*-5 and PC 34:1*n*-5, respectively (**Figure 6**). Alternatively, KRAS mutation could be increasing expression or activity of the fatty acid synthase enzyme FASN leading to increased partitioning towards other pathways such as desaturation. However, given that the protumorigenic mutation is also present in the parental cell line and no significant presence of an *n*-5 isomer is observed by either technique, there is evidently more complexity in the biochemical pathways leading to the changes in the mutant cell line. Further studies on a wider range of cancerous cell lines would be required to reveal the diversity in the pathways that would lead to the changes in isomer distribution observed here.

CONCLUSIONS

Across both simple and complex lipid standards, *de novo* analysis of both OzID and UVPD spectra using established rules for these ion activation modalities have shown the potential for false positive assignments of site(s) of unsaturation in shotgun lipidomics. Importantly, these competing fragmentation processes can be understood and appropriate caution or correction applied in the biological interpretation of results. Specifically, in the presence of lipids with abundant *n-x* double bond(s), care needs to be taken in the assignment of low abundant OzID signals corresponding to *n*-(*x*+1) double bonds as these can arise from secondary reactions of the unsaturated Criegee ions deriving from oxidative cleavage of the *n-x* bond. These findings urge particular caution to be exercised at longer OzID reaction times (or higher ozone concentrations) where secondary reactions can become more prominent. Even under such conditions however, the secondary reaction products appear to rarely exceed 1% of the *n-x* signal for *cis*-double bonds, confirming prior suggestions of a conservative 1.5% threshold for distinguishing artifactual signals from true con-

tributions from isomeric lipids.[71] In the case of UVPD, consistent *n*-(*x*±1) false positives were observed with significant product ion abundances (up to 5% of the *n*-*x* signal). While the precise mechanism giving rise to these artifacts and its dependence on irradiation time and laser power remains to be determined, the relatively consistent pattern of ion abundance *ca*. 3:100:2 (*x*-1:*x*:*x*+1) may assist in discriminating true- from false-positive assignments in a biological context. The comparable performance obtained using these techniques on the same platform suggests that, in a shotgun analysis, unsaturated lipids should be detected by *both* UVPD and OzID to provide confirmation of structural assignments, particularly in cases where the putative sites of unsaturation are inconsistent with canonical lipid metabolism. Comparing the relative abundances of selected isomeric lipids across isogenic parental, wildtype and mutant CRC cell lines, significant remodeling of oleic (18:1*n*-9) and *cis*-vaccenic (18:1*n*-7) acid-containing phosphatidylcholine 16:0_18:1 is observed due to the pro-tumorigenic KRAS mutation, but not in anti-tumorigenic MEK knockouts. Both techniques also detect formation of a PC 32:1*n*-5 isomer in the KRAS mutant cell line, suggesting desaturation is out-competing fatty acyl chain elongation. The results obtained from UVPD and OzID may therefore provide insights into oncogenic cellular lipid synthesis and metabolism that are inaccessible with tandem mass spectrometry methods based on collisional activation.

ASSOCIATED CONTENT

Supporting Information

The Supporting Information is available free of charge on the ACS Publications website.

Lipid standard structures and exact masses, schematic diagram of instrument modification. Predicted neutral losses/gains for OzID and UVPD of monounsaturated FAs and PCs. HCD-MS/MS spectra and sum of diagnostic ions for OzID (10ms) and UVPD (50 and 100 shots) of dilithiated FAs. Mechanisms for isomerization of the double bond and formation of *sn*-diagnostic fragment ions by OzID and UVPD. CID-OzID-MS/MS and UVPD-MS/MS spectra for references PC 36:2 and for parental DLD1 CRC line PC 32:1. Normalized abundances of molecular lipids and double bond positional lipids in DLD1 CRC lines. OzID-MS/MS and UVPD-MS/MS spectra for KRAS mutant DLD1 CRC line PC 32:1 and PC 34:1. Proposed biochemical pathways to rationalize formation of non-canonical *n*-5 carbon-carbon double bonds (DOC).

Data availability

The data presented here are available for download from the Queensland University of Technology *Research Data Finder* archive at: https://doi.org/10.25912/RDF_1720443901543

AUTHOR INFORMATION

Corresponding Authors

Gavin E. Reid - *School of Chemistry, University of Melbourne, Parkville, VIC 3010, Australia; Department of Biochemistry and Pharmacology, University of Melbourne, Parkville, VIC 3010, Australia; Bio21 Molecular Science and Biotechnology Institute, University of Melbourne, Parkville, VIC 3010, Australia;* orcid.org/0000-0002-9675-1444
Email: gavin.reid@unimelb.edu.au

Stephen J. Blanksby - *Central Analytical Research Facility, Queensland University of Technology, Brisbane, QLD 4001, Australia; School of Chemistry and Physics, Queensland University of Technology, Brisbane, QLD 4001, Australia;* orcid.org/0000-0002-8560-756X
Email: stephen.blanksby@qut.edu.au

David L. Marshall - *Central Analytical Research Facility, Queensland University of Technology, Brisbane, QLD 4001, Australia;* orcid.org/0000-0002-1711-2338
Email: d20.marshall@qut.edu.au

Author

Samuel C. Brydon - *School of Chemistry and Physics, Queensland University of Technology, Brisbane, QLD 4001, Australia;* orcid.org/0000-0002-8939-0249

Berwyck L.J. Poad - *Central Analytical Research Facility, Queensland University of Technology, Brisbane, QLD 4001, Australia; School of Chemistry and Physics, Queensland University of Technology, Brisbane, QLD 4001, Australia;* orcid.org/0000-0002-0420-6116

Mengxuan Fang - *School of Chemistry, University of Melbourne, Parkville, VIC 3010, Australia;*

Yepy H. Rustam - *Department of Biochemistry and Pharmacology, University of Melbourne, Parkville, VIC 3010, Australia;* orcid.org/0000-0002-1298-9034

Reuben S.E. Young - *Molecular Horizons and School of Chemistry and Molecular Bioscience, University of Wollongong, Wollongong, NSW 2522, Australia;* orcid.org/0000-0003-0620-3362

Dmitri Mouradov - *Personalized Oncology Division, The Walter and Eliza Hall Institute of Medical Research, Parkville, VIC 3052, Australia*; orcid.org/0000-0001-8149-816X

Oliver M. Sieber - *Personalized Oncology Division, The Walter and Eliza Hall Institute of Medical Research, Parkville, VIC 3052, Australia*; orcid.org/0000-0001-9480-0786

Todd W. Mitchell - *Molecular Horizons and School of Medical, Indigenous and Health Sciences, University of Wollongong, Wollongong, NSW 2522, Australia;* orcid.org/0000-0002-1372-9963

Author Contributions

All authors have given approval to the final version of the manuscript.

Methodology: B.L.J.P., D.M., O.M.S, G.E.R., S.J.B. Investigation: B.L.J.P., M.F, Y.H.R. Data analysis; S.C.B., R.S.E.Y. Writing – original draft preparation: S.C.B. Writing – review and editing: S.C.B., R.S.E.Y., G.E.R., S.J.B., D.L.M. Conceptualization: G.E.R., S.J.B., T.W.M. Supervision: G.E.R., S.J.B. Project administration: G.E.R., S.J.B. Funding acquisition: O.M.S., G.E.R., S.J.B., T.W.M.

Notes

The authors declare no competing financial interest.

ACKNOWLEDGMENT

S.J.B. and T.W.M. are grateful to the Australian Research Council for funding (DP190101486). G.E.R. and O.M.S., acknowledge funding from the National Health and Medical Research Council (APP1156778) and from the Australian Research Council (DP190102464), and G.E.R. acknowledges infrastructure funding through the Australian Research Council (LE200100117). The authors are grateful for instrument access, training and support provided through the Central Analytical Research Facility (QUT) and the Mass Spectrometry and Proteomics facility at Bio21 and The University of Melbourne.

REFERENCES

1. Pikó, P.; Pál, L.; Szűcs, S.; Kósa, Z.; Sándor, J.; Ádány, R., Obesity-Related Changes in Human Plasma Lipidome Determined by the Lipidyzer Platform. *Biomolecules* **2021,** *11* (2), 326.
2. Tan, Y. M.; Gao, Y.; Teo, G.; Koh, H. W. L.; Tai, E. S.; Khoo, C. M.; Choi, K. P.; Zhou, L.; Choi, H., Plasma Metabolome and Lipidome Associations with Type 2 Diabetes and Diabetic Nephropathy. *Metabolites* **2021,** *11* (4), 228.
3. Huynh, K.; Lim, W. L. F.; Giles, C.; Jayawardana, K. S.; Salim, A.; Mellett, N. A.; Smith, A. A. T.; Olshansky, G.; Drew, B. G.; Chatterjee, P.; Martins, I.; Laws, S. M.; Bush, A. I.; Rowe, C. C.; Villemagne, V. L.; Ames, D.; Masters, C. L.; Arnold, M.; Nho, K.; Saykin, A. J.; Baillie, R.; Han, X.; Kaddurah-Daouk, R.; Martins, R. N.; Meikle, P. J., Concordant peripheral lipidome signatures in two large clinical studies of Alzheimer's disease. *Nat. Commun.* **2020,** *11* (1), 5698.
4. Liu, Y.; Thalamuthu, A.; Mather, K. A.; Crawford, J.; Ulanova, M.; Wong, M. W. K.; Pickford, R.; Sachdev, P. S.; Braidy, N., Plasma lipidome is dysregulated in Alzheimer's disease and is associated with disease risk genes. *Transl. Psychiatry* **2021,** *11* (1), 344.
5. Röhrig, F.; Schulze, A., The multifaceted roles of fatty acid synthesis in cancer. *Nat. Rev. Cancer* **2016,** *16* (11), 732-749.
6. Butler, L. M.; Perone, Y.; Dehairs, J.; Lupien, L. E.; de Laat, V.; Talebi, A.; Loda, M.; Kinlaw, W. B.; Swinnen, J. V., Lipids and cancer: Emerging roles in pathogenesis, diagnosis and therapeutic intervention. *Adv. Drug Deliv. Rev.* **2020,** *159*, 245-293.
7. Perrotti, F.; Rosa, C.; Cicalini, I.; Sacchetta, P.; Del Boccio, P.; Genovesi, D.; Pieragostino, D., Advances in Lipidomics for Cancer Biomarkers Discovery. *Int. J. Mol. Sci.* **2016,** *17* (12), 1992.
8. Yan, G.; Li, L.; Zhu, B.; Li, Y., Lipidome in colorectal cancer. *Oncotarget* **2016,** *7* (22), 33429-39.
9. Ecker, J.; Benedetti, E.; Kindt, A. S. D.; Höring, M.; Perl, M.; Machmüller, A. C.; Sichler, A.; Plagge, J.; Wang, Y.; Zeissig, S.; Shevchenko, A.; Burkhardt, R.; Krumsiek, J.; Liebisch, G.; Janssen, K.-P., The Colorectal Cancer Lipidome: Identification of a Robust Tumor-Specific Lipid Species Signature. *Gastroenterology* **2021,** *161* (3), 910-923.e19.
10. Vriens, K.; Christen, S.; Parik, S.; Broekaert, D.; Yoshinaga, K.; Talebi, A.; Dehairs, J.; Escalona-Noguero, C.; Schmieder, R.; Cornfield, T.; Charlton, C.; Romero-Pérez, L.; Rossi, M.; Rinaldi, G.; Orth, M. F.; Boon, R.; Kerstens, A.; Kwan, S. Y.; Faubert, B.; Méndez-Lucas, A.; Kopitz, C. C.; Chen, T.; Fernandez-Garcia, J.; Duarte, J. A. G.; Schmitz, A. A.; Steigemann, P.; Najimi, M.; Hägebarth, A.; Van Ginderachter, J. A.; Sokal, E.; Gotoh, N.; Wong, K.-K.; Verfaillie, C.; Derua, R.; Munck, S.; Yuneva, M.; Beretta, L.; DeBerardinis, R. J.; Swinnen, J. V.; Hodson, L.; Cassiman, D.; Verslype, C.; Christian, S.; Grünewald, S.; Grünewald, T. G. P.; Fendt, S.-M., Evidence for an alternative fatty acid desaturation pathway increasing cancer plasticity. *Nature* **2019,** *566* (7744), 403-406.
11. Centenera, M. M.; Scott, J. S.; Machiels, J.; Nassar, Z. D.; Miller, D. C.; Zinonos, I.; Dehairs, J.; Burvenich, I. J. G.; Zadra, G.; Chetta, P. M.; Bango, C.; Evergren, E.; Ryan, N. K.; Gillis, J. L.; Mah, C. Y.; Tieu, T.; Hanson, A. R.; Carelli, R.; Bloch, K.; Panagopoulos, V.; Waelkens, E.; Derua, R.; Williams, E. D.; Evdokiou, A.; Cifuentes-Rius, A.; Voelcker, N. H.; Mills, I. G.; Tilley, W. D.; Scott, A. M.; Loda, M.; Selth, L. A.; Swinnen, J. V.; Butler, L. M., ELOVL5 Is a Critical and Targetable Fatty Acid Elongase in Prostate Cancer. *Cancer Res.* **2021,** *81* (7), 1704-1718.
12. Martinez-Seara, H.; Róg, T.; Pasenkiewicz-Gierula, M.; Vattulainen, I.; Karttunen, M.; Reigada, R., Interplay of Unsaturated Phospholipids and Cholesterol in Membranes: Effect of the Double-Bond Position. *Biophys. J.* **2008,** *95* (7), 3295-3305.
13. Renne, M. F.; de Kroon, A. I., The role of phospholipid molecular species in determining the physical properties of yeast membranes. *FEBS Lett.* **2018,** *592* (8), 1330-1345.
14. Brenna, J. T.; Kothapalli, K. S., New understandings of the pathway of long-chain polyunsaturated fatty acid biosynthesis. *Curr. Opin. Clin. Nutr. Metab. Care* **2022,** *25* (2), 60-66.
15. Guillou, H.; Zadravec, D.; Martin, P. G.; Jacobsson, A., The key roles of elongases and desaturases in mammalian fatty acid metabolism: Insights from transgenic mice. *Prog. Lipid Res.* **2010,** *49* (2), 186-199.
16. Ma, X.; Chong, L.; Tian, R.; Shi, R.; Hu, T. Y.; Ouyang, Z.; Xia, Y., Identification and quantitation of lipid C=C location isomers: A shotgun lipidomics approach enabled by photochemical reaction. *Proc. Natl. Acad. Sci. U.S.A.* **2016,** *113* (10), 2573-2578.
17. Paine, M. R. L.; Poad, B. L. J.; Eijkel, G. B.; Marshall, D. L.; Blanksby, S. J.; Heeren, R. M. A.; Ellis, S. R., Mass Spectrometry Imaging with Isomeric Resolution Enabled by Ozone-Induced Dissociation. *Angew. Chem. Int. Ed.* **2018,** *57* (33), 10530-10534.
18. Klein, D. R.; Feider, C. L.; Garza, K. Y.; Lin, J. Q.; Eberlin, L. S.; Brodbelt, J. S., Desorption electrospray ionization coupled with ultraviolet photodissociation for characterization of phospholipid isomers in tissue sections. *Anal. Chem.* **2018,** *90* (17), 10100-10104.
19. Liu, X.; Jiao, B.; Cao, W.; Ma, X.; Xia, Y.; Blanksby, S. J.; Zhang, W.; Ouyang, Z., Development of a Miniature Mass Spectrometry System for Point-of-Care Analysis of Lipid Isomers Based on Ozone-Induced Dissociation. *Anal. Chem.* **2022,** *94* (40), 13944-13950.
20. Ge, L.; Gordon, J. S.; Hsuan, C.; Stenn, K.; Prouty, S. M., Identification of the Δ-6 Desaturase of Human Sebaceous Glands: Expression and Enzyme Activity. *J. Invest. Dermatol.* **2003,** *120* (5), 707-714.
21. Ferreri, C.; Sansone, A.; Buratta, S.; Urbanelli, L.; Costanzi, E.; Emiliani, C.; Chatgilialoglu, C., The n-10 Fatty Acids Family in the Lipidome of Human Prostatic Adenocarcinoma Cell Membranes and Extracellular Vesicles. *Cancers* **2020,** *12* (4), 900.
22. Young, R. S. E.; Bowman, A. P.; Williams, E. D.; Tousignant, K. D.; Bidgood, C. L.; Narreddula, V. R.; Gupta, R.; Marshall, D. L.; Poad, B. L. J.; Nelson, C. C.; Ellis, S. R.; Heeren, R. M. A.; Sadowski, M. C.; Blanksby, S. J., Apocryphal FADS2 activity promotes fatty acid diversification in cancer. *Cell Rep.* **2021,** *34* (6), 108738.
23. Kothapalli, K. S. D.; Park, H. G.; Kothapalli, N. S. L.; Brenna, J. T., FADS2 function at the major cancer hotspot 11q13 locus alters fatty acid metabolism in cancer. *Prog. Lipid Res.* **2023,** *92*, 101242.
24. Blanksby, S. J.; Mitchell, T. W., Advances in mass spectrometry for lipidomics. *Annu. Rev. Anal. Chem.* **2010,** *3*, 433-465.
25. Rustam, Y. H.; Reid, G. E., Analytical Challenges and Recent Advances in Mass Spectrometry Based Lipidomics. *Anal. Chem.* **2018,** *90* (1), 374-397.
26. Hsu, F.-F.; Turk, J., Electrospray ionization with low-energy collisionally activated dissociation tandem mass spectrometry of glycerophospholipids: Mechanisms of fragmentation and structural characterization. *J. Chromatogr. B* **2009,** *877* (26), 2673-2695.
27. Yang, K.; Zhao, Z.; Gross, R. W.; Han, X., Identification and Quantitation of Unsaturated Fatty Acid Isomers by Electrospray Ionization Tandem Mass Spectrometry: A Shotgun Lipidomics Approach. *Anal. Chem.* **2011,** *83* (11), 4243-4250.
28. Young, R. S. E.; Flakelar, C. L.; Narreddula, V. R.; Jekimovs, L. J.; Menzel, J. P.; Poad, B. L. J.; Blanksby, S. J., Identification of Carbon-Carbon Double Bond Stereochemistry in Unsaturated Fatty Acids by Charge-Remote Fragmentation of Fixed-Charge Derivatives. *Anal. Chem.* **2022,** *94* (46), 16180-16188.
29. Pittenauer, E.; Allmaier, G., The renaissance of high-energy CID for structural elucidation of complex lipids: MALDI-TOF/RTOF-MS of alkali cationized triacylglycerols. *J. Am. Soc. Mass. Spectrom.* **2009,** *20* (6), 1037-1047.
30. Hsu, F.-F.; Turk, J., Structural characterization of unsaturated glycerophospholipids by multiple-stage linear ion-trap mass spectrometry with electrospray ionization. *J. Am. Soc. Mass. Spectrom.* **2008,** *19* (11), 1681-1691.
31. Pham, H. T.; Ly, T.; Trevitt, A. J.; Mitchell, T. W.; Blanksby, S. J., Differentiation of Complex Lipid Isomers by Radical-Directed Dissociation Mass Spectrometry. *Anal. Chem.* **2012,** *84* (17), 7525-7532.

32. Murphy, R. C., *Tandem mass spectrometry of lipids: molecular analysis of complex lipids*. Royal Society of Chemistry: 2014.
33. Ryan, E.; Reid, G. E., Chemical derivatization and ultrahigh resolution and accurate mass spectrometry strategies for "shotgun" lipidome analysis. *Acc. Chem. Res.* **2016,** *49* (9), 1596-1604.
34. Xia, F.; Wan, J.-B., Chemical derivatization strategy for mass spectrometry-based lipidomics. *Mass Spectrom. Rev.* **2023,** *42* (1), e21729.
35. Wang, D.; Xiao, H.; Lv, X.; Chen, H.; Wei, F., Mass Spectrometry Based on Chemical Derivatization Has Brought Novel Discoveries to Lipidomics: A Comprehensive Review. *Crit. Rev. Anal. Chem.* **2023**, 1-32.
36. Campbell, J. L.; Baba, T., Near-Complete Structural Characterization of Phosphatidylcholines Using Electron Impact Excitation of Ions from Organics. *Anal. Chem.* **2015,** *87* (11), 5837-5845.
37. Jones, J. W.; Thompson, C. J.; Carter, C. L.; Kane, M. A., Electron-induced dissociation (EID) for structure characterization of glycerophosphatidylcholine: determination of double-bond positions and localization of acyl chains. *J. Mass Spectrom.* **2015,** *50* (12), 1327-1339.
38. Born, M.-E. N.; Prentice, B. M., Structural elucidation of phosphatidylcholines from tissue using electron induced dissociation. *Int. J. Mass spectrom.* **2020,** *452*, 116338.
39. Shenault, D. S. M.; McLuckey, S. A.; Franklin, E. T., Localization of cyclopropyl groups and alkenes within glycerophospholipids using gas-phase ion/ion chemistry. *J. Mass Spectrom.* **2023,** *58* (4), e4913.
40. Mitchell, T. W.; Pham, H.; Thomas, M. C.; Blanksby, S. J., Identification of double bond position in lipids: From GC to OzID. *J. Chromatogr. B* **2009,** *877* (26), 2722-2735.
41. Holcapek, M.; Ekroos, K., *Mass Spectrometry for Lipidomics: Methods and Applications*. John Wiley & Sons: 2023.
42. Heiles, S., Advanced tandem mass spectrometry in metabolomics and lipidomics—methods and applications. *Anal. Bioanal. Chem.* **2021,** *413* (24), 5927-5948.
43. Feng, Y.; Chen, B.; Yu, Q.; Li, L., Identification of double bond position isomers in unsaturated lipids by m-CPBA epoxidation and mass spectrometry fragmentation. *Anal. Chem.* **2019,** *91* (3), 1791-1795.
44. Yang, T.; Tang, S.; Kuo, S.-T.; Freitas, D.; Edwards, M.; Wang, H.; Sun, Y.; Yan, X., Lipid Mass Tags via Aziridination for Probing Unsaturated Lipid Isomers and Accurate Relative Quantification. *Angew. Chem. Int. Ed.* **2022,** *61* (39), e202207098.
45. Wan, Q.; Xiao, Y.; Feng, G.; Dong, X.; Nie, W.; Gao, M.; Meng, Q.; Chen, S., Visible-light-activated aziridination reaction enables simultaneous resolving of C=C bond location and the sn-position isomers in lipids. *Chin. Chem. Lett.* **2023**, 108775.
46. Cerrato, A.; Cavaliere, C.; Laganà, A.; Montone, C. M.; Piovesana, S.; Sciarra, A.; Taglioni, E.; Capriotti, A. L., First Proof of Concept of a Click Inverse Electron Demand Diels–Alder Reaction for Assigning the Regiochemistry of Carbon–Carbon Double Bonds in Untargeted Lipidomics. *Anal. Chem.* **2024**.
47. Ma, X.; Xia, Y., Pinpointing double bonds in lipids by Paternò-Büchi reactions and mass spectrometry. *Angew. Chem. Int. Ed.* **2014,** *53* (10), 2592-2596.
48. Xie, X.; Xia, Y., Analysis of conjugated fatty acid isomers by the paterno-buchi reaction and trapped ion mobility mass spectrometry. *Anal. Chem.* **2019,** *91* (11), 7173-7180.
49. Murphy, R. C.; Okuno, T.; Johnson, C. A.; Barkley, R. M., Determination of Double Bond Positions in Polyunsaturated Fatty Acids Using the Photochemical Paternò-Büchi Reaction with Acetone and Tandem Mass Spectrometry. *Anal. Chem.* **2017,** *89* (16), 8545-8553.
50. Wäldchen, F.; Becher, S.; Esch, P.; Kompauer, M.; Heiles, S., Selective phosphatidylcholine double bond fragmentation and localisation using Paternò–Büchi reactions and ultraviolet photodissociation. *Analyst* **2017,** *142* (24), 4744-4755.
51. Ma, X.; Zhang, W.; Li, Z.; Xia, Y.; Ouyang, Z., Enabling High Structural Specificity to Lipidomics by Coupling Photochemical Derivatization with Tandem Mass Spectrometry. *Acc. Chem. Res.* **2021,** *54* (20), 3873-3882.
52. Klein, D. R.; Brodbelt, J. S., Structural Characterization of Phosphatidylcholines Using 193 nm Ultraviolet Photodissociation Mass Spectrometry. *Anal. Chem.* **2017,** *89* (3), 1516-1522.
53. Ryan, E.; Nguyen, C. Q. N.; Shiea, C.; Reid, G. E., Detailed Structural Characterization of Sphingolipids via 193 nm Ultraviolet Photodissociation and Ultra High Resolution Tandem Mass Spectrometry. *J. Am. Soc. Mass. Spectrom.* **2017,** *28* (7), 1406-1419.
54. Williams, P. E.; Klein, D. R.; Greer, S. M.; Brodbelt, J. S., Pinpointing Double Bond and sn-Positions in Glycerophospholipids via Hybrid 193 nm Ultraviolet Photodissociation (UVPD) Mass Spectrometry. *J. Am. Chem. Soc.* **2017,** *139* (44), 15681-15690.
55. Macias, L. A.; Feider, C. L.; Eberlin, L. S.; Brodbelt, J. S., Hybrid 193 nm ultraviolet photodissociation mass spectrometry localizes cardiolipin unsaturations. *Anal. Chem.* **2019,** *91* (19), 12509-12516.
56. Buenger, E. W.; Reid, G. E., Shedding light on isomeric FAHFA lipid structures using 213 nm ultraviolet photodissociation mass spectrometry. *Eur. J. Mass Spectrom.* **2020,** *26* (5), 311-323.
57. Fang, M.; Rustam, Y.; Palmieri, M.; Sieber, O. M.; Reid, G. E., Evaluation of ultraviolet photodissociation tandem mass spectrometry for the structural assignment of unsaturated fatty acid double bond positional isomers. *Anal. Bioanal. Chem.* **2020,** *412* (10), 2339-2351.
58. Blevins, M. S.; Shields, S. W. J.; Cui, W.; Fallatah, W.; Moser, A. B.; Braverman, N. E.; Brodbelt, J. S., Structural Characterization and Quantitation of Ether-Linked Glycerophospholipids in Peroxisome Biogenesis Disorder Tissue by Ultraviolet Photodissociation Mass Spectrometry. *Anal. Chem.* **2022,** *94* (37), 12621-12629.
59. Kralj, T.; Nuske, M.; Hofferek, V.; Sani, M.-A.; Lee, T.-H.; Separovic, F.; Aguilar, M.-I.; Reid, G. E., Multi-omic analysis to characterize metabolic adaptation of the E. coli lipidome in response to environmental stress. *Metabolites* **2022,** *12* (2), 171.
60. Thomas, M. C.; Mitchell, T. W.; Harman, D. G.; Deeley, J. M.; Nealon, J. R.; Blanksby, S. J., Ozone-Induced Dissociation: Elucidation of Double Bond Position within Mass-Selected Lipid Ions. *Anal. Chem.* **2008,** *80* (1), 303-311.
61. Poad, B. L. J.; Pham, H. T.; Thomas, M. C.; Nealon, J. R.; Campbell, J. L.; Mitchell, T. W.; Blanksby, S. J., Ozone-induced dissociation on a modified tandem linear ion-trap: Observations of different reactivity for isomeric lipids. *J. Am. Soc. Mass. Spectrom.* **2010,** *21* (12), 1989-1999.
62. Pham, H. T.; Maccarone, A. T.; Campbell, J. L.; Mitchell, T. W.; Blanksby, S. J., Ozone-Induced Dissociation of Conjugated Lipids Reveals Significant Reaction Rate Enhancements and Characteristic Odd-Electron Product Ions. *J. Am. Soc. Mass Spectrom.* **2013,** *24* (2), 286-296.
63. Pham, H. T.; Maccarone, A. T.; Thomas, M. C.; Campbell, J. L.; Mitchell, T. W.; Blanksby, S. J., Structural characterization of glycerophospholipids by combinations of ozone- and collision-induced dissociation mass spectrometry: the next step towards "top-down" lipidomics. *Analyst* **2014,** *139* (1), 204-214.
64. Marshall, D. L.; Pham, H. T.; Bhujel, M.; Chin, J. S. R.; Yew, J. Y.; Mori, K.; Mitchell, T. W.; Blanksby, S. J., Sequential Collision- and Ozone-Induced Dissociation Enables Assignment of Relative Acyl Chain Position in Triacylglycerols. *Anal. Chem.* **2016,** *88* (5), 2685-2692.
65. Poad, B. L. J.; Green, M. R.; Kirk, J. M.; Tomczyk, N.; Mitchell, T. W.; Blanksby, S. J., High-Pressure Ozone-Induced Dissociation for Lipid Structure Elucidation on Fast Chromatographic Timescales. *Anal Chem* **2017,** *89* (7), 4223-4229.
66. Marshall, D. L.; Criscuolo, A.; Young, R. S. E.; Poad, B. L. J.; Zeller, M.; Reid, G. E.; Mitchell, T. W.; Blanksby, S. J., Mapping Unsaturation in Human Plasma Lipids by Data-Independent Ozone-Induced Dissociation. *J. Am. Soc. Mass. Spectrom.* **2019,** *30* (9), 1621-1630.
67. Claes, B. S. R.; Bowman, A. P.; Poad, B. L. J.; Young, R. S. E.; Heeren, R. M. A.; Blanksby, S. J.; Ellis, S. R., Mass Spectrometry Imaging of Lipids with Isomer Resolution Using High-Pressure Ozone-Induced Dissociation. *Anal. Chem.* **2021,** *93* (28), 9826-9834.

68. Young, R. S. E.; Bowman, A. P.; Tousignant, K. D.; Poad, B. L. J.; Gunter, J. H.; Philp, L. K.; Nelson, C. C.; Ellis, S. R.; Heeren, R. M. A.; Sadowski, M. C.; Blanksby, S. J., Isomeric lipid signatures reveal compartmentalized fatty acid metabolism in cancer. *J. Lipid Res.* **2022,** *63* (6).

69. Klein, D. R.; Blevins, M. S.; Macias, L. A.; Douglass, M. V.; Trent, M. S.; Brodbelt, J. S., Localization of Double Bonds in Bacterial Glycerophospholipids Using 193 nm Ultraviolet Photodissociation in the Negative Mode. *Anal. Chem.* **2020,** *92* (8), 5986-5993.

70. Hancock, S. E.; Maccarone, A. T.; Poad, B. L. J.; Trevitt, A. J.; Mitchell, T. W.; Blanksby, S. J., Reaction of ionised steryl esters with ozone in the gas phase. *Chem. Phys. Lipids* **2019,** *221*, 198-206.

71. Menzel, J. P.; Young, R. S. E.; Benfield, A. H.; Scott, J. S.; Wongsomboon, P.; Cudlman, L.; Cvačka, J.; Butler, L. M.; Henriques, S. T.; Poad, B. L. J.; Blanksby, S. J., Ozone-enabled fatty acid discovery reveals unexpected diversity in the human lipidome. *Nat. Commun.* **2023,** *14* (1), 3940.

72. Ross, D. H.; Lee, J.-Y.; Bilbao, A.; Orton, D. J.; Eder, J. G.; Burnet, M. C.; Deatherage Kaiser, B. L.; Kyle, J. E.; Zheng, X., LipidOz enables automated elucidation of lipid carbon–carbon double bond positions from ozone-induced dissociation mass spectrometry data. *Commun. Chem.* **2023,** *6* (1), 74.

73. Morrison, L. J.; Parker, W. R.; Holden, D. D.; Henderson, J. C.; Boll, J. M.; Trent, M. S.; Brodbelt, J. S., UVliPiD: A UVPD-Based Hierarchical Approach for De Novo Characterization of Lipid A Structures. *Anal. Chem.* **2016,** *88* (3), 1812-1820.

74. Michael, J. A.; Young, R. S. E.; Balez, R.; Jekimovs, L. J.; Marshall, D. L.; Poad, B. L. J.; Mitchell, T. W.; Blanksby, S. J.; Ejsing, C. S.; Ellis, S. R., Deep Characterisation of the sn-Isomer Lipidome Using High-Throughput Data-Independent Acquisition and Ozone-Induced Dissociation. *Angew. Chem. Int. Ed.* **2024,** *63* (9), e202316793.

75. Damiani, T.; Bonciarelli, S.; Thallinger, G. G.; Koehler, N.; Krettler, C. A.; Salihoğlu, A. K.; Korf, A.; Pauling, J. K.; Pluskal, T.; Ni, Z.; Goracci, L., Software and Computational Tools for LC-MS-Based Epilipidomics: Challenges and Solutions. *Anal. Chem.* **2023,** *95* (1), 287-303.

76. Bowden, J. A.; Heckert, A.; Ulmer, C. Z.; Jones, C. M.; Koelmel, J. P.; Abdullah, L.; Ahonen, L.; Alnouti, Y.; Armando, A. M.; Asara, J. M.; Bamba, T.; Barr, J. R.; Bergquist, J.; Borchers, C. H.; Brandsma, J.; Breitkopf, S. B.; Cajka, T.; Cazenave-Gassiot, A.; Checa, A.; Cinel, M. A.; Colas, R. A.; Cremers, S.; Dennis, E. A.; Evans, J. E.; Fauland, A.; Fiehn, O.; Gardner, M. S.; Garrett, T. J.; Gotlinger, K. H.; Han, J.; Huang, Y.; Neo, A. H.; Hyötyläinen, T.; Izumi, Y.; Jiang, H.; Jiang, H.; Jiang, J.; Kachman, M.; Kiyonami, R.; Klavins, K.; Klose, C.; Köfeler, H. C.; Kolmert, J.; Koal, T.; Koster, G.; Kuklenyik, Z.; Kurland, I. J.; Leadley, M.; Lin, K.; Maddipati, K. R.; McDougall, D.; Meikle, P. J.; Mellett, N. A.; Monnin, C.; Moseley, M. A.; Nandakumar, R.; Oresic, M.; Patterson, R.; Peake, D.; Pierce, J. S.; Post, M.; Postle, A. D.; Pugh, R.; Qiu, Y.; Quehenberger, O.; Ramrup, P.; Rees, J.; Rembiesa, B.; Reynaud, D.; Roth, M. R.; Sales, S.; Schuhmann, K.; Schwartzman, M. L.; Serhan, C. N.; Shevchenko, A.; Somerville, S. E.; St. John-Williams, L.; Surma, M. A.; Takeda, H.; Thakare, R.; Thompson, J. W.; Torta, F.; Triebl, A.; Trötzmüller, M.; Ubhayasekera, S. J. K.; Vuckovic, D.; Weir, J. M.; Welti, R.; Wenk, M. R.; Wheelock, C. E.; Yao, L.; Yuan, M.; Zhao, X. H.; Zhou, S., Harmonizing lipidomics: NIST interlaboratory comparison exercise for lipidomics using SRM 1950-Metabolites in Frozen Human Plasma. *J. Lipid Res.* **2017,** *58* (12), 2275-2288.

77. Burla, B.; Arita, M.; Arita, M.; Bendt, A. K.; Cazenave-Gassiot, A.; Dennis, E. A.; Ekroos, K.; Han, X.; Ikeda, K.; Liebisch, G.; Lin, M. K.; Loh, T. P.; Meikle, P. J.; Orešič, M.; Quehenberger, O.; Shevchenko, A.; Torta, F.; Wakelam, M. J. O.; Wheelock, C. E.; Wenk, M. R., MS-based lipidomics of human blood plasma: a community-initiated position paper to develop accepted guidelines. *J. Lipid Res.* **2018,** *59* (10), 2001-2017.

78. Poad, B. L. J.; Zheng, X.; Mitchell, T. W.; Smith, R. D.; Baker, E. S.; Blanksby, S. J., Online Ozonolysis Combined with Ion Mobility-Mass Spectrometry Provides a New Platform for Lipid Isomer Analyses. *Anal. Chem.* **2018,** *90* (2), 1292-1300.

79. Sanders, J. D.; Shields, S. W.; Escobar, E. E.; Lanzillotti, M. B.; Butalewicz, J. P.; James, V. K.; Blevins, M. S.; Sipe, S. N.; Brodbelt, J. S., Enhanced Ion Mobility Separation and Characterization of Isomeric Phosphatidylcholines Using Absorption Mode Fourier Transform Multiplexing and Ultraviolet Photodissociation Mass Spectrometry. *Anal. Chem.* **2022,** *94* (10), 4252-4259.

80. Liebisch, G.; Fahy, E.; Aoki, J.; Dennis, E. A.; Durand, T.; Ejsing, C. S.; Fedorova, M.; Feussner, I.; Griffiths, W. J.; Köfeler, H.; Merrill, A. H.; Murphy, R. C.; O'Donnell, V. B.; Oskolkova, O.; Subramaniam, S.; Wakelam, M. J. O.; Spener, F., Update on LIPID MAPS classification, nomenclature, and shorthand notation for MS-derived lipid structures. *J. Lipid Res.* **2020,** *61* (12), 1539-1555.

81. The nomenclature of lipids (recommendations 1976). *J. Lipid Res.* **1978,** *19* (1), 114-128.

82. Shirasawa, S.; Furuse, M.; Yokoyama, N.; Sasazuki, T., Altered growth of human colon cancer cell lines disrupted at activated Ki-ras. *Science* **1993,** *260* (5104), 85-88.

83. Lydic, T. A.; Busik, J. V.; Reid, G. E., A monophasic extraction strategy for the simultaneous lipidome analysis of polar and nonpolar retina lipids. *J. Lipid Res.* **2014,** *55* (8), 1797-1809.

84. Brown, S. H. J.; Mitchell, T. W.; Blanksby, S. J., Analysis of unsaturated lipids by ozone-induced dissociation. *Biochem. Biophys. Acta Mol. Cell Biol. Lipids* **2011,** *1811* (11), 807-817.

85. Baker, J.; Aschmann, S. M.; Arey, J.; Atkinson, R., Reactions of stabilized criegee intermediates from the gas-phase reactions of O_3 with selected alkenes. *Int. J. Chem. Kinet.* **2002,** *34* (2), 73-85.

86. Collin, G. J., Photochemistry of Simple Olefins: Chemistry of Electronic Excited States or Hot Ground State? In *Advances in Photochemistry*, John Wiley & Sons: 1988; Vol. 14, pp 135-176.

87. Bollinger, J. G.; Rohan, G.; Sadilek, M.; Gelb, M. H., LC/ESI-MS/MS detection of FAs by charge reversal derivatization with more than four orders of magnitude improvement in sensitivity. *J. Lipid Res.* **2013,** *54* (12), 3523-3530.

88. Canez, C. R.; Li, L., Investigation of the Effects of Labware Contamination on Mass Spectrometry-Based Human Serum Lipidome Analysis. *Anal. Chem.* **2024,** *96* (21), 8373-8380.

89. Hsu, F.-F.; Turk, J., Distinction among isomeric unsaturated fatty acids as lithiated adducts by electrospray ionization mass spectrometry using low energy collisionally activated dissociation on a triple stage quadrupole instrument. *J. Am. Soc. Mass. Spectrom.* **1999,** *10* (7), 600-612.

90. Hsu, F.-F.; Turk, J., Elucidation of the Double-Bond Position of Long-Chain Unsaturated Fatty Acids by Multiple-Stage Linear Ion-Trap Mass Spectrometry with Electrospray Ionization. *J. Am. Soc. Mass. Spectrom.* **2008,** *19* (11), 1673-1680.

91. Crockett, J. S.; Gross, M. L.; Christie, W. W.; Holman, R. T., Collisional activation of a series of homoconjugated octadecadienoic acids with fast atom bombardment and tandem mass spectrometry. *J. Am. Soc. Mass. Spectrom.* **1990,** *1* (2), 183-191.

92. Cheng, C.; Gross, M. L., Applications and mechanisms of charge-remote fragmentation. *Mass Spectrom. Rev.* **2000,** *19* (6), 398-420.

93. Harvey, D. J., A new charge-associated mechanism to account for the production of fragment ions in the high-energy CID spectra of fatty acids. *J. Am. Soc. Mass. Spectrom.* **2005,** *16* (2), 280-290.

94. Vu, N.; Brown, J.; Giles, K.; Zhang, Q., Ozone-induced dissociation on a traveling wave high-resolution mass spectrometer for determination of double-bond position in lipids. *Rapid Commun. Mass Spectrom.* **2017,** *31* (17), 1415-1423.

95. Lee, H. Y.; Kislov, V. V.; Lin, S. H.; Mebel, A. M.; Neumark, D. M., An ab Initio/RRKM Study of Product Branching Ratios in the Photodissociation of Buta-1, 2-and-1, 3-dienes and But-2-yne at 193 nm. *Chem. Eur. J.* **2003,** *9* (3), 726-740.

96. Kirschbaum, C.; Greis, K.; Polewski, L.; Gewinner, S.; Schöllkopf, W.; Meijer, G.; von Helden, G.; Pagel, K., Unveiling Glycerolipid Fragmentation by Cryogenic Infrared Spectroscopy. *J. Am. Chem. Soc.* **2021,** *143* (36), 14827-14834.

97. Becher, S.; Berden, G.; Martens, J.; Oomens, J.; Heiles, S., IRMPD Spectroscopy of [PC (4:0/4:0) + M]+ (M = H, Na, K) and Corresponding CID Fragment Ions. *J. Am. Soc. Mass. Spectrom.* **2021,** *32* (12), 2874-2884.

98. Kozlowski, R. L.; Mitchell, T. W.; Blanksby, S. J., Separation and Identification of Phosphatidylcholine Regioisomers by Combining Liquid Chromatography with a Fusion of Collision- and Ozone-Induced Dissociation. *Eur. J. Mass Spectrom.* **2015,** *21* (3), 191-200.

99. Menendez, J. A.; Lupu, R., Fatty acid synthase and the lipogenic phenotype in cancer pathogenesis. *Nat. Rev. Cancer* **2007,** *7* (10), 763-777.

100. Currie, E.; Schulze, A.; Zechner, R.; Walther, T. C.; Farese, R. V., Cellular fatty acid metabolism and cancer. *Cell Metab.* **2013,** *18* (2), 153-161.

101. Salita, T.; Rustam, Y. H.; Mouradov, D.; Sieber, O. M.; Reid, G. E., Reprogrammed Lipid Metabolism and the Lipid-Associated Hallmarks of Colorectal Cancer. *Cancers* **2022,** *14* (15), 3714.

102. Pakiet, A.; Kobiela, J.; Stepnowski, P.; Sledzinski, T.; Mika, A., Changes in lipids composition and metabolism in colorectal cancer: a review. *Lipids Health Dis.* **2019,** *18* (1), 29.

103. Wang, C.; Fakih, M., Targeting KRAS in colorectal cancer. *Curr. Oncol. Rep.* **2021,** *23*, 1-10.

104. Ricoult, S. J.; Yecies, J. L.; Ben-Sahra, I.; Manning, B. D., Oncogenic PI3K and K-Ras stimulate de novo lipid synthesis through mTORC1 and SREBP. *Oncogene* **2016,** *35* (10), 1250-1260.

105. Mossmann, D.; Park, S.; Hall, M. N., mTOR signalling and cellular metabolism are mutual determinants in cancer. *Nat. Rev. Cancer* **2018,** *18* (12), 744-757.

Table of Contents (TOC)